Julio, 2014

Universidad de Oviedo

Departamento de Química Física y Analítica

Área de Química Física

Chemical Interactions in the Low Pressure Phase of Gas Clathrate Hydrates

Fernando Izquierdo Ruiz

European Master in Theoretical Chemistry and Computational Modelling

D. Ángel Martín Pendás, Coordinador del Máster Europeo en Química Teórica y Modelización Computacional,

CERTIFICA:

Que el trabajo titulado "**Chemical Interactions in the Low Pressure Phase of Gas Clathrate Hydrates**" ha sido realizado en el Departamento de Química Física y Analítica de la Universidad de Oviedo por Fernando Izquierdo Ruiz bajo la dirección de Jose Manuel Recio Muñiz y Julia Contreras García con el fin de optar al título que otorga el Máster Europeo en Química Teórica y Modelización Computacional.

Oviedo, 17 de julio de 2014
El Coordinador del Máster.

Fdo.: Ángel Martín Pendás.

D. José Manuel Recio Muñiz, Catedrático de Química Física del Departamento de Química Física y Analítica de la Universidad de Oviedo y **Dña. Julia Contreras García**, Full Researcher (CR2) del CNRS en el Laboratoire de Chimie Théorique de la Université Pierre et Marie Curie (París, Francia),

CERTIFICAN:

Que el trabajo titulado "**Chemical Interactions in the Low Pressure Phase of Gas Clathrate Hydrates**" ha sido realizado bajo su dirección por Fernando Izquierdo Ruiz, constituyendo su Tesis de Máster, cuya presentación autorizan.

Oviedo, 17 de julio de 2014

Fdo.: José Manuel Recio Muñiz   Julia Contreras García.

AGRADECIMIENTOS

A Michi, Julia, Olga y Alberto, por todo lo que me ayudan siempre que se lo pido y por tener infinita paciencia conmigo. A Mónica, por toda su ayuda en París. A Mamel, porque desde el exilio sigue pendiente de nosotros.

A mi familia, incluyendo tíos, primos y abuelo, por su apoyo incondicional e inquebrantable.

A mis amigos, los de Oviedo, los del Máster y los de Madrid, porque siempre saben levantarme el ánimo en todo momento o ponerme en mi sitio cuando lo merezco.

A Serra, por que me aguanta y me apoya siempre con una sonrisa.

A los compañeros del laboratorio. A los profesores del grupo de Química Cuántica: Victor Luaña, Evelio Francisco, José Manuel Recio, Ángel Martín Pendás, Manuel Flórez, Ruth Franco, Aurora Costales, Miguel Ángel Salvadó y Pilar Pertierra. Por su ayuda siempre que se les pide y sus conocimientos. A Victor Luaña por dejarme tomar prestadas algunas figuras de sus diapositivas.

A la FICYT, ya que me dan el soporte monetario para continuar con la Tesis Doctoral. Al proyecto MALTA-Consolider y al proyecto CTQ2012-38599-C02-01 por la financiación.

CONTENTS

LIST OF TABLES

LIST OF FIGURES

CAPÍTULO 1

INTRODUCCIÓN

Los clatratos son estructuras cristalinas que contienen disposiciones atómicas con forma de cavidades o jaulas susceptibles de alojar gases en su interior. Si el armazón está constituido por moléculas de agua reciben el nombre de clatratos hidratos de gas o simplemente hidratos de gas. Estos minerales se forman en sistemas a alta presión y baja temperatura, por lo que en la Tierra se asocian con ambientes en condiciones extremas. Debido sus características específicas, derivadas básicamente de la estructura, la investigación de los clatratos es relevante en campos del conocimiento tan dispares como la planetología, la geomicrobiología, el estudio del origen de la vida o la explotación de recursos naturales.

Con respecto al primer campo mencionado, aunque directamente no se han detectado clatratos de gas fuera de La Tierra, ya hace más de 40 años que se propuso su presencia en el Sistema Solar, desde Marte hasta los satélites de hielo y los cometas [1, 2]. La razón principal de que no se hayan localizado aún es que la instrumentación incluida en las misiones espaciales hasta el momento no ha sido la adecuada para diferenciar estos hielos de otras fases de agua pura.

Sin embargo, se sabe que tanto los componentes químicos (agua y gases) como las condiciones físicas apropiadas para su formación (alta presión, baja temperatura) se alcanzan en diferentes ambientes planetarios como las cortezas heladas y reservorios acuosos profundos de las lunas de los planetas gigantes del Sistema Solar. Se ha sugerido, por ejemplo, que los clatratos son la causa de la señal de CO_2 asociada a los depósitos de materiales oscuros de Europa, también que son la fuente para el CH_4 que se detecta en la atmósfera de Titán, así como el origen de algunos de los volátiles de la pluma de Encélado (por ejemplo CO_2, CH_4 y N_2). En nuestro planeta debemos señalar también la existencia de grandes reservorios de hidrógeno y de metano alojados en clatratos de agua en los fondos marinos y debajo del permafrost. Se han llevado a cabo además numerosas investigaciones experimentales y teóricas dirigidas específicamente a la caracterización estructural de estos sistemas, al estudio de la energética de la ocupación de las cavidades con gases puros o mezclas incluyendo hidrocarburos y al análisis de sus espectros Raman e infrarrojo [3, 4, 5].

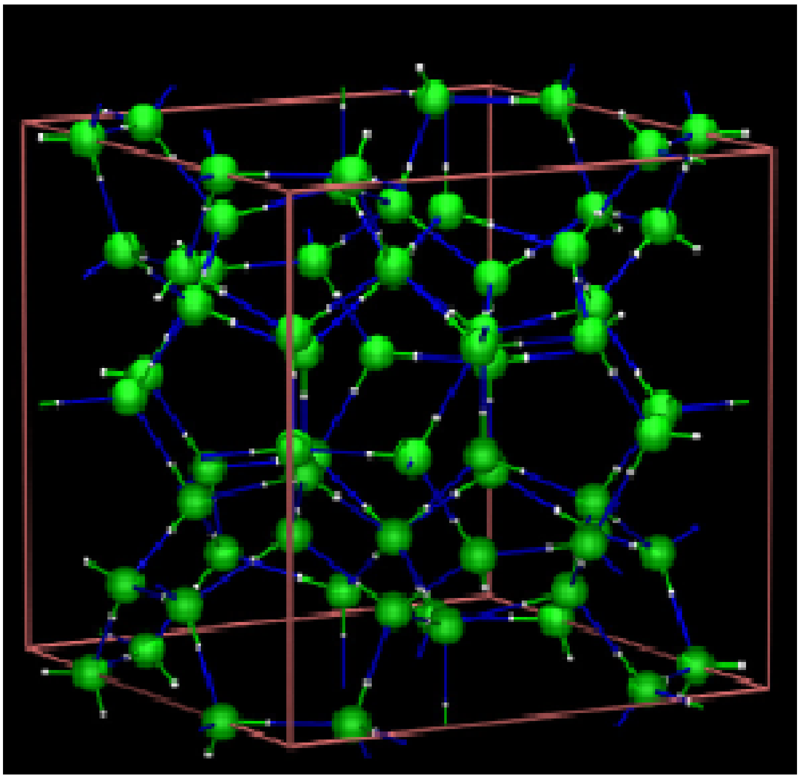

Figura 1.1: Celda unidad del armazón del clatrato correspondiente a la estructura sI. Las bolas grandes verdes representan átomos de O, las bolas pequeñas blancas representan átomos de H, las líneas de unión verdes representan enlaces O-H covalentes y las líneas de unión azules representan enlaces de puente de hidrógeno O-H.

El polimorfismo inducido por presión es uno de los fenómenos fundamentales en los hidratos de gas. Además de las diferentes fases del hielo, se encuentran otras fases, denominadas clatratos y FIS (*Filled Ice Structure*, Estructura de hielo relleno) [6], con estabilidades en diversos rangos de presión y temperatura [7]. Los clatratos se pueden clasificar en las estructuras sI , sII (cúbicas) y sH (hexagonal) [6, 7]. En este trabajo nos centraremos en la fase clatrato de tipo sI, menos compleja que las fases sII y sH, aunque con un número de átomos en su celda unidad mucho mayor que en las estructuras FIS. El tamaño y número de cavidades o cajas cambian de una fase a otra, y por tanto la propia estructura, al aumentar la presión hidrostática [7]. Esto restringe la naturaleza de los gases potenciales que puedan alojarse en el interior de cada uno de los polimorfos. Las cavidades tienen formas poliédricas con caras mayoritariamente pentagonales y hexagonales, como se puede apreciar en la estructura cúbica denominada sI de la Fig. 1.1. Los gases son apolares o con baja polaridad (H_2, Br_2, CO_2, CH_4, C_2H_6, C_3H_8, etc.) [6]. El grado de saturación de las distintas cavidades y la posibilidad de que una misma estructura aloje distintos gases (clatratos mixtos) determina su comportamiento. Es por tanto crucial la caracterización estructural y espectral para conocer cómo la química y física de los hidratos de gas evoluciona en los distintos ambientes termodinámicos en los que pueden encontrarse.

Los clatratos hidratos de gas presentan además muchas propiedades muy similares a algunas de las fases sólidas del agua. La identificación de aquellas propiedades que sirvan para detectar la presencia de clatratos [8], y de los efectos sobre el ambiente que produce la formación y destrucción de estos minerales, son de gran interés de la exploración espacial del futuro próximo. Los rangos de estabilidad termodinámica (presión y temperatura), las propiedades de transporte (conductividad térmica) y la espectroscopía vibracional (Raman fundamentalmente) deben ser investigados con detalle pues pueden ser utilizados como sensores diferenciadores o identificadores de la presencia de los clatratos de agua. Para avanzar en esta línea, se requiere en todos los casos un mayor conocimiento de las interacciones entre las moléculas gaseosas (*guest*) y el armazón del hidrato (*host*). Las simulaciones computacionales con métodos químico cuánticos constituyen herramientas valiosas para acceder a esta información y merecen comentarse con más detalle ya que forman la parte fundamental de nuestra investigación.

En primer lugar tenemos que señalar que el armazón tridimensional de los clatratos hidratos está exclusivamente sostenido y cohesionado gracias a las denominadas interacciones no covalentes (NCI, del inglés non-covalent interactions). Las NCIs son débiles si las comparamos con los enlaces covalentes, y son mas díficiles de tratar desde el punto de vista mecánico-cuántico. En las simulaciones con metodologías basadas en la teoría del funcional de la densidad no se tratan explicitamente las contribuciones energéticas de dispersión [9, 10]. Aunque ha habido progresos recientes en el tratamiento de estos términos de dispersión, está claro que todavía hay grandes dificultades para describir con éxito los sistemas agregados finitos o sólidos basados en el agua [11]. De hecho, podemos decir que tanto las simulaciones estáticas como las dinámicas en modelos acuosos utilizando cálculos DFT constituyen uno de los retos de mayor magnitud para la química computacional, siendo actualmente una materia de intenso debate [12].

La dificultad es mayor si pretendemos simular con éxito el comportamiento de los clatratos hidratos sometidos a presión hidrostática. Aunque hagamos uso de métodos DFT con correcciones de dispersión, el problema se agudiza ya que en estas simulaciones se combina la presencia de transferencia de carga a través de los enlaces de hidrógeno con cambios en las contribuciones electrostáticas y de dispersión inducidos por la presión. Sabemos, por ejemplo, que los funcionales de la densidad con correcciones de dispersión pierden precisión si se pretenden describir geometrías comprimidas de dimeros gasesos [13] o efectos de transferencia de carga [14]. En los últimos años, el modelo XDM (del inglés exchange-hole dipole moment) propuesto por Becke y Johnson [15] ha proporcionado energías de interacción muy precisas tanto en clusters en fase gaseosa [16] como en fases condensadas [17, 18, 19]. Comparado con correcciones de dispersión más simples [20], XDM sí se muestra sensible a cambios en el entorno químico [10], por lo que este modelo constituye la elección apropiada para estudiar interacciones *guest-host*, efectos de presión y propiedades espectroscópicas de vibración en sistemas de clatratos hidratos.

Nuestro estudio teórico y computacional se sitúa en el campo de las simulaciones estáticas de primeros principios. Aunque es conocido que los efectos dinámicos juegan un papel fundamental en muchas propiedades si la temperatura no es muy baja, consideramos que la capacidad descriptiva de la aproximación estática proporciona información valiosa y necesaria previa a las simulaciones dinámicas. Nos centraremos aquí en cinco tipos de resultados. Todos ellos para los clatratos hidratos de metano y dióxido de carbono en la fase cúbica estable a baja presión denominada *sI*. Utilizaremos en ocasiones los símbolos CH_4@sI y CO_2@sI para referirnos a estos sistemas.

Los primeros resultados están dedicados a la estructura geométrica de equilibrio de los clatratos vacíos y alojando las moléculas gaseosas en todas sus cavidades. Estudiaremos con detalle las orientaciones preferentes de las dos moléculas en los dos tipos de cavidades que presenta esta estructura. Los segundos resultados se dedican al estudio de la energética asociada a la saturación de las cavidades con cada uno de los dos tipos de moléculas gaseosas. Los efectos de la presión en la estructura y estabilidad, y la determinación de la ecuación de estado estática constituyen la tercera parte de nuestra investigación. Hasta aquí debemos señalar que todas las simulaciones se llevarán a cabo con metodologás para sistemas cristalinos periódicos. En cuarto lugar llevaremos a cabo un estudio pormenorizado de las interacciones guest-host en los dos sistemas, CH_4@sI y CO_2@sI. Aquí, ademas de la función de onda del sistema cristalino, utilizaremos las soluciones obtenidas de cálculos de cluster o sistemas finitos. Este análisis se lleva a cabo utilizando el gradiente reducido de la densidad electrónica y permite visualizar y conocer con detalle la naturaleza de las interacciones no covalentes. Finalmente, presentaremos resultados de los cálculos de las vibraciones de estos sistemas utilizando clusters constituidos por los dos tipos de cajas.

El documento se estructura en otros tres capítulos siguiendo una presentación tradicional. En el siguiente, se describen los aspectos computacionales de las metodologías utilizadas incluyendo una breve introducción de los fundamentos teóricos. En el tercer capítulo se analizan los resultados obtenidos organizados en cuatro apartados: estructura y ecuación de estado, energética y estabilidad de la ocupación de las cavidades, discusión de las interacciones no covalentes y estudio preliminar de las vibraciones moleculares. La Tesis de Máster finaliza con un resumen de las conclusiones más relevantes del estudio y algunas ideas del trabajo que se pretende llevar a cabo en el futuro. Para cumplir la normativa del Máster en Química Teórica y Modelización Computacional, el resto del documento, salvo las conclusiones, estará escrito en inglés.

CHAPTER 2

COMPUTATIONAL MODELLING

This chapter is intended to present a brief summary of theoretical aspects and computational details related to the computational modelling of the gas clathrate hydrates under study in this investigation. In the following five sections, we will cover the crystallographic description and geometrical structure of these systems, the electronic structure calculations of periodic and finite cluster models, the analysis of chemical interactions through the reduced density gradient, the evaluation of equation of state parameters, and the determination of vibrational frequencies of finite clusters.

2.1 Geometric structure

To define appropriately a system of interest, either a molecule or a solid, it is important to describe its symmetry. There are two types of symmetry. One that arises in all systems called point symmetry, in which all the symmetry elements coincide at one point. And another one that only exists only in periodic systems, either in one, two or three dimensions, which is the translational symmetry. By combining these two symmetries, it is possible to obtain all the spatial groups of symmetry in periodic systems. In the following sections, we will briefly describe the periodic symmetry.

2.1.1 Basic crystallography

In this section, several basic concepts used to describe periodic systems are presented. Firstly, it is important to note that solids are treated as ideal, without any defect, and infinite systems.

A **crystal lattice** is an infinite network of points that have translational symmetry in one or more dimensions. A **Bravais lattice** is a crystal lattice that fulfills the condition that from each point of the lattice the environment is exactly the same. The **molecular motif** can be combined with the crystal lattice to form the structure of the solid. In Figure 2.1 an example is showed.

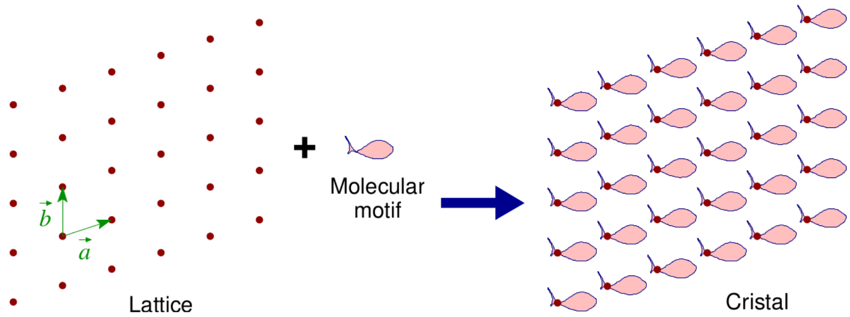

Figure 2.1: Example of lattice and molecular motif

It is possible to define a vector between two of the lattice points. These are **lattice vectors**. A special type of lattice vectors are the **primitive vectors**, lattice vectors that describe any lattice point with only integer vector translations. Then, the positions of the points in the lattice can be defined as a linear combination of linearly independent primitive vectors in the way $\vec{R} = \sum_i^2 n_i \vec{a}_i$, where i is the index over the number of dimensions, 2 in this example, n_i must be an integer and $\vec{a}_i$ are primitive vectors. They allow to simplify the notation. In the previous example we take the basis $\{\vec{a}_i\}_{i=1,2}$, the position of a lattice point can be expressed as (n_1, n_2).

The parallelepiped defined by independent lattice vectors is called the **unit cell** and its repetition along all the space reproduces the whole crystal. There are infinite ways to define the basis of the structure and, thus, infinite unit cells. However, a usual way to define the unit cell is to take the primitive vectors as basis. These define the **primitive cell**, which is the smallest cell that is possible to create in the crystal. It contains only one lattice point. In addition, it is possible to define larger cells that contain more than one lattice point, these are called **centered cells**. The use of centered cells implies that fractional coordinates will appear to define the position of certain points. Centered cells are used for convenience.

The geometry of the cell can be defined also with the cell parameters. These parameters are the length of the edges and the angles between them. In a general way they are defined as $a, b, c, \alpha, \beta, \gamma$, being α the angle formed by b and c and so on (see Figure 2.2). Then, we can define the seven crystallographic systems and the fourteen Bravais lattices, as they are summarized in Table 2.1.

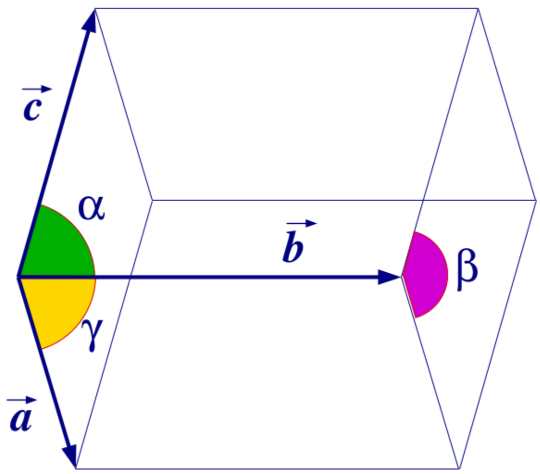

Figure 2.2: Cell parameters and relationship between edges and angles

The types of Bravais lattices are classified according to the centering of the cell. They can be either primitive (P), body centered (I), face centered (F) or one face centered (B or C). The trigonal cell has two different settings, hexagonal (H) or rhombohedral (R). When the Bravais lattices are combined with the 32 allowed point groups, which exclude symmetry axis of order 5 or greater than 6 in crystalline solids, the 230 space groups arise.

There are, also, another symmetry operations, called non-symmorphic operations, which include fractional translations. They are the screw axes and the glide planes. 73 of the 230 systems are symmorphic groups.

Cryst. System	Symmetry	Cell Parameters	Bravais latt.
Cubic	4 C_3 axis	$a = b = c,\ \alpha = \beta = \gamma = 90°$	P, I, F
Hexagonal	a 6 order axis	$a = b,\ \alpha = \beta = 90°,\ \gamma = 120°$	P
Trigonal (H)	a 3 order axis	$a = b,\ \alpha = \beta = 90°,\ \gamma = 120°$	R
Trigonal (R)	a 3 order axis	$a = b = c,\ \alpha = \beta = \gamma$	R
Tetragonal	a 4 order axis	$a = b,\ \alpha = \beta = \gamma = 90°$	P, I
Orthorhombic	3 2 order axis	$\alpha = \beta = \gamma = 90°$	P, I, F, C
Monoclinic	a 2 order axis	$\alpha = \gamma = 90°$	P, B, C
Triclinic	no symmetry	none	P

Table 2.1: Crystal systems and Bravais lattices

The application of symmetry operations to any point inside the unit cell produces equivalent positions of that point. These are called **Wyckoff positions** and are characterized by its multiplicity and a label to differentiate them from each other when they have different symmetries. Next, we present the crystallographic description of our chemical system using these concepts.

According to the review of Loveday [7], the sI clathrate studied in this work has a cubic spatial group $Pm\bar{3}n$ (223). The protons in the cage framework are disordered, similarly to what happens in most ice phases. The specific positions of the hydrogen atoms are not unambiguously available from X-ray experiments. We decided to assign hydrogens to oxygens preserving the water molecule geometry. The hydrogens atoms are added following the ice rules (four atoms around each oxygen, two closer and two farther) and make them to follow as much as possible the original symmetry. We expect the hydrogen position to affect the total energy via cooperative effects, but we also estimate that these are relative small compared to pressure effects.

The unit cell has 46 molecules of water that form eight cages. Two of these cages are formed by pentagonal faces (5^{12}) that make a stretched dodecahedron. We call them pentagonal or P cages. The other six cages are hexagonal truncated trapezohedrons, or tetrakaidecahedrons ($5^{12}6^2$). We call them hexagonal or H cages. In Table 2.2, we collect the positions of the non-equivalent oxygen atoms of the sI unit cell. We include the positions of the centers of the two clathrate cavities. Notice that the carbon atoms of the guest gas molecule CH_4 and CO_2 are situated at these centers [7].

Atom	x	y	z	Wykcoff pos.
O1	0	0.5	0.25	6c
O2	0.183	0.183	0.183	16i (x,x,x)
O3	0	0.310	0.123	24k (0,y,z)
P center	0	0	0	2a
H center	0	0.25	0.5	6d

Table 2.2: Experimental parameters of sI type structure

In Figure 2.3 there is a representation of the crystalline structure and the two cages. The red balls represent oxygens and the white balls represent hydrogens. It is important to note that once the coordinates of the hydrogens are specifically fixed the structure the symmetry can be lowered up to the triclinic P1 space group. Either in the experiments (where hydrogen atoms do not occupy specific coordinates) or in the simulations (hydrogen atoms are unequivocally localized) the clathrate network is mainly supported by the oxygen sub-lattice frame.

2.2 Electronic structure

In this section the general aspects of the electronic structure calculations will be explained for both cluster and periodic systems. To determine the behaviour of molecular sized systems the main methodology is Quantum Mechanics. This branch of science tries to solve the Schrödinger equation to obtain the properties of the system under study.

$$\hat{H}\Psi = E\Psi, \tag{2.1}$$

where $\hat{H}$ is the Hamiltonian of the system, Ψ is the wavefunction of the system and E is the energy of the system. Unfortunately, the Schrödinger equation can

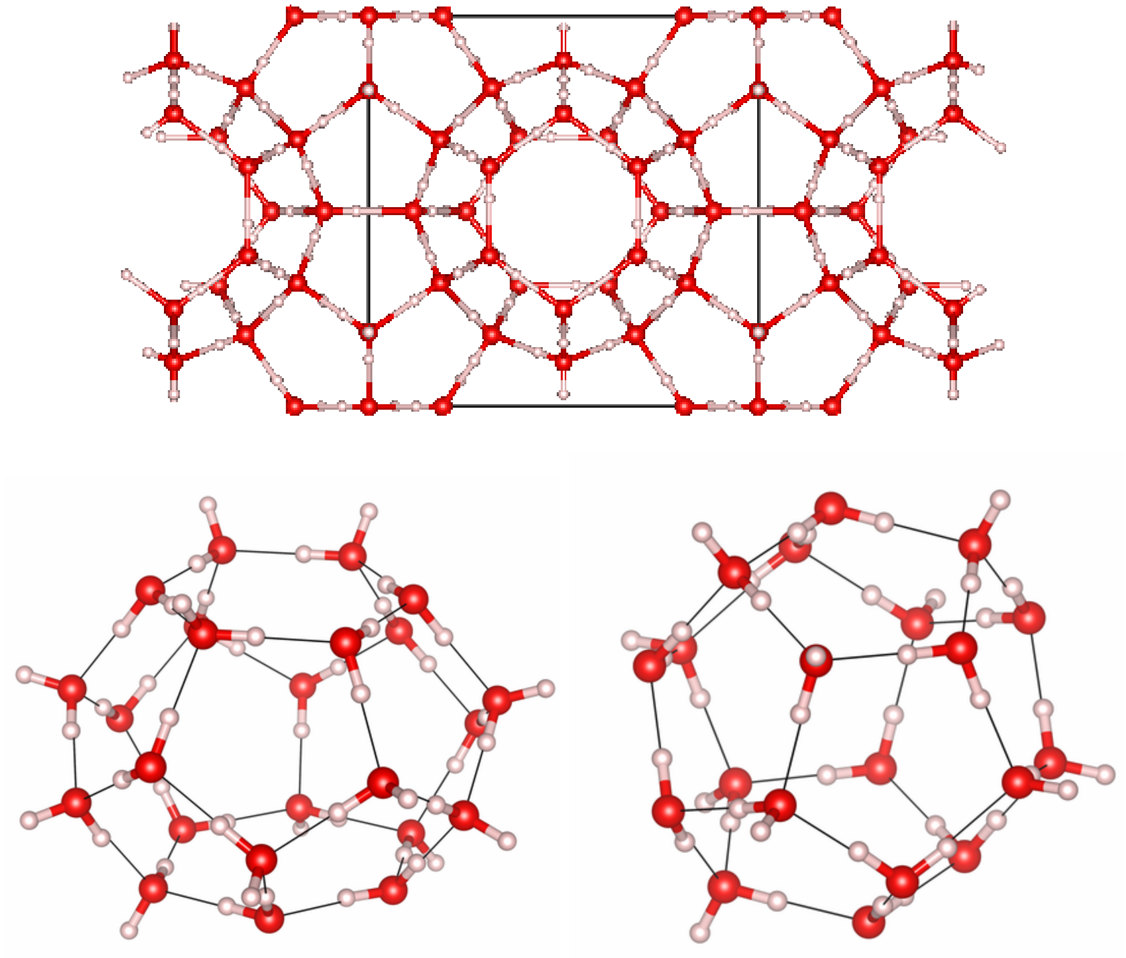

Figure 2.3: Crystalline structure of clathrate sI (top), H (left) and P (right) cages

not be exactly solved for systems with more than one electron. This problem forces us to rely in approximations to simplify that equation.

An approximation commonly used in all the *ab initio* simulations is the Born-Oppenhemier (B-O) approach [21]. This approximation assumes that the movement of the electrons and the nuclei are decoupled due to the huge difference of mass between them. In addition, the system is considered in the static approximation, considering the system at 0 K and without zero point vibrational energy (*i.e.* frozen).

One of the first quantum mechanical method was the one developed by Hartree and Fock around 1930. It is called the Self-Consistent-Field (SCF) method. It takes advantage of the variational theorem. The SCF method became really efficient once Roothan developed the Linear Combination of Atomic Orbitals (LCAO) approximation [22, 23], that transformed the integro-differential equation problem into a algebraic problem. After the SCF method was implemented several other so called wavefunction methods have been implemented during the years (MP2, CI, CC, MRSCF) to try to overcome the main problem of accurately describing the electron correlation.

As an alternative to wavefunction methods there are the so called Density Functional Theory (DFT) methods. Instead of using the wavefunction of the system in *n* dimensions, DFT uses the electronic density (that depends only in 3 variables) to solve the Schrödinger equation, as Hohenberg and Kohn (H-k) proved [24] and Kohn and Sham (K-S) implemented [25]:

$$\frac{\delta E[\rho]}{\delta \rho} = \mu, \qquad \hat{H}_{KS} = \hat{T} + V_{ext}. \tag{2.2}$$

The first one is the fundamental equation of DFT obtained by H-K theorems, where E is the energy, ρ is the electronic density and μ is the chemical potential of the electrons. The second one is the expression of the K-S Hamiltonian that relates the real system of interacting electrons with one of non-interacting electrons under an external potential V_{ext} that generates the same electron density ($\hat{T}$ is the kinetic energy of the electrons). These approximations allow to perform a SCF procedure so it is possible to recover part of the electronic correlation (if the exact exchange and correlation functional were known all the electron correlation would be recovered) at a lower computational cost than in post-HF calculations. The two main drawbacks of DFT methodology are: i) some of the approximations in the implementation are not variational and ii) the exact exchange and correlation functional is not known so approximations to this functional are needed which lead to propose a variety of functionals for this term.

The approximations to the exchange and correlation functional are classified as if they were rungs of a ladder [26]. The classification divides the functionals into LDA (Local Density Approximation, relates the energy with the density), GGA (Generalized Gradient Approximation, adding a term that depends on the gradient), meta-GGA (adding the kinetic energy density or the laplacian) and hybrid functionals (including part of the exact exchange). Recently, newer double hybrid functionals and other solutions (like random phase approximation) are becoming more important.

Our simulations follow DFT methodologies and B-O and the static approximations. The calculation of energies and geometries of gas clathrate hydrates systems can be divided, from a practical point of view, in two categories: finite (or cluster) calculations, in which a part of the system composed of a finite number of atoms is isolated, and periodic calculations, where the clathrate is assumed to be periodic and infinite in the three dimensions. The former allows the use of a broader array of computational techniques including highly-correlated wave-function theory methods and density functionals that use an admixture of exact exchange. The latter are usually a more faithful representation of a crystalline solid. They incorporate very-long-range electrostatic interactions, but they are mostly limited to density-functional methodologies using semilocal functionals unless very simple systems are considered. In our work, we have employed a combination of finite and periodic electronic structure methodologies.

2.2.1 Finite systems

Regarding the finite systems, we performed two kinds of calculations using the ubiquitous atom-centered gaussian function basis sets as implemented in the Gaussian09 code [27]. The first set comprises the calculation of the association (binding) energies between the host (a clathrate cage) and the guest (CH_4 or CO_2). The second type of calculation is aimed at the vibrational properties of the host and guest, and are discussed in section 2.5.

These calculations were carried out using the B3LYP [28, 29] and the PW86PBE [30, 31, 32] functional (made of Perdew-Wang 1986 exchange and Perdew-Burke-Ernzerhof correlation). The former is a global hybrid functional that mixes 20% exact exchange with the Becke 88 (B88) exchange functional[33], combined with Lee-Yang-Parr correlation[29]. B3LYP is the most widely-used functional in chemistry[34], owing to its balanced description of reaction kinetics and excellent thermochemistry. PW86PBE is a semilocal Generalized-Gradient Approximation (GGA) functional that has been shown to provide a good description of the Pauli repulsive wall in non-covalent interactions [35, 36], and it is in consequence a natural choice for our study.

The binding energy calculations were carried out using the aug-cc-pVDZ basis set of Dunning et al. [37]. Although not as critical for DFT as it is for correlated wave-function-theory calculations, the choice of basis may affect the resulting binding energies and care must be taken to correct for basis set incompleteness. The origin of basis set superposition errors (BSSE) has been shown to come from the description of the intermolecular density regions [38]. The overall effect of BSSE on non-covalent interactions is to overestimate binding energies, which is caused by the poor description of the fragments relative to the whole. This is particularly true in the case of hydrogen-bonded systems, where there is a non-negligible intermolecular density in the hydrogen bond region owing to intermolecular charge transfer and induction effects. In order to account for BSSE, we have employed the traditional Counterpoise (CP) method [39], proposed by Boys and Bernardi. In a CP-corrected calculation, the binding energy is computed as the difference between the whole and the fragment energies, where the monomers have been calculated using the basis-set of the dimer. It has been shown [40] that in hydrogen-bonded systems the CP correction overcorrects (in general) and that a reliable strategy is to take only half of the CP correction. That is, the binding energy is calculated as the average between the "normal" and the CP-corrected binding energy. As in our case all hydrogen bonds are always included in one of the fragments, this average is not needed.

Non-covalent interactions, such as those arising in clathrate hydrates, are not well described by common density functionals such as PW86PBE or B3LYP [9, 10]. This happens because of the missing dispersion effects, which are long-range correlation effects not accounted for by semilocal (or hybrid) functionals. Scores of corrections and new functionals for non-covalent interactions have been proposed over the last decade [9], and in this work we are going to focus on two: the exchange-hole dipole moment (XDM) model [41, 42, 15] and Grimme's D2 [20] and D3 [43, 44] corrections. Both XDM and Grimme's dispersion corrections add a dispersion energy term to the electronic energy calculated by some "popular" functional, such as PW86PBE or B3LYP (in the following, the base functional). Therefore, the total energy is:

$$E_{\text{total}} = E_{\text{base}} + E_{\text{disp}}, \tag{2.3}$$

where the dispersion correction has a pairwise summation expression that runs over all pairs of atoms in the system:

$$E_{\text{disp}} = -\sum_{A>B}\sum_{n}\frac{C_n^{\text{AB}} f_n(R_{AB})}{R_{AB}^n}. \tag{2.4}$$

The sum goes over all pairs of atoms A and B and makes use of the interatomic distances R_{AB}. The C_n quantitites are called the dispersion (or interaction) coefficients, and can be calculated, for instance, using time-dependent density-functional theory (TDDFT) or wave-function-theory methods. The f_n object is a one-dimensional scalar function called the damping function that goes to zero when $R_{AB} \to 0$ and to one in the $R_{AB} \to \infty$ limit. The role of this damping function is to deactivate the dispersion correction at short range and account for the errors introduced by the approximation involved in using a pairwise summation. In dispersion-corrected DFT, the damping function also fulfills the role of correcting for spurious or erratic behavior from the base functional in the description of the non-dispersive part of the non-covalent interactions. The sum in equation above goes, in principle, to infinite order, but in practice it is usually truncated at $n = 10$ because higher-order coefficients give a negligible contribution to the dispersion energy [45]. Hence, the sum is restricted to the leading dipole-dipole $n = 6$ term that characterizes dispersion long-range behavior and the higher-order dipole-quadrupole ($n = 8$) and quadrupole-quadrupole ($n = 10$) terms, that do represent a non-negligible amount of dispersion energy.

The basic objects in the formula above are the interaction coefficients C_n for $n = 6$, 8, and 10. XDM and the D2 and D3 corrections are, in the end, methods for calculating dispersion coefficients. In XDM, the C_n are calculated non-empirically using a method based on the Becke-Roussel (BR) exchange-hole model [46]. The dispersion interaction between two neutral separated atoms (or molecules or fragments) is represented by the electrostatic interaction of the dipoles formed by the electrons and their associated exchange holes. The spherically-averaged exchange hole in the BR model is represented by a simple exponential at a certain distance from the reference point, and has three parameters that are found by imposing known exact constraints that the exact exchange hole is known to fulfill. By using the BR model, the calculation of the dipole-dipole interaction between two electrons at given points can be calculated using only the density and the Kohn-Sham kinetic energy density, hence making XDM a meta-GGA approximation to the dispersion coefficients. The dispersion coefficients in XDM have been shown to be accurate to about 10%, and they can be calculated for any order of the interaction (n in the equation above) [45]. XDM has been shown to provide excellent accuracy when treating systems in the gas-phase [16] as well as in condensed phases [17, 18, 19]

There are two popular versions of Grimme's dispersion correction: D2 [20] and the more-modern D3 [43, 44]. The former is the most popular dispersion correction today and was essential in showing that pairwise-based dispersion-corrected DFT is an accurate method for the description of non-covalent interactions. In the D2 method, the dispersion sum goes only up to $n = 6$ and the dispersion coefficients are constant and do not depend on the chemical environment (as they should). Despite these deficiencies, D2 achieves impressive accuracy in the treatment of small dimers [44] and is very much used in the modeling of condensed phases and surfaces as well [47]. Two very popular functionals that use the D2 correction in gas-phase calculations are B97D [20] and the range-separated hybrid functional ωB97XD[48].

The D3 correction tries to fix the chief shortcomings of D2 (interaction coefficients independent of the chemical environment and missing higher-order energy terms) and is quickly gaining popularity and being incorporated in most software packages. The interaction coefficients in D3 are calculated from an internal database and modified according to a recipe that estimates the effect of the chemical environment on an atom from the geometry alone. The dispersion energy expression includes the $n = 8$ term, but scaled by an empirical coefficient. Even though the simplicity of D2 is sacrificed in D3, the latter still depends on the geometry alone (although in a very complex way) and does improve the treatment of dispersion according to standard benchmark tests [44].

In our guest-host interaction energy calculations, we considered the two types of cages present in the s-I clathrate hydrate (P and H) and inserted a guest molecule in them, as shown in Figure 2.4. We considered the same water cage geometry in the crystal, because relaxing the geometry in the gas-phase would be unphysical given the extended cooperative hydrogen bonding effects in the hydrate. Several orientations of the carbon dioxide molecule inside were considered, obtained by rotating the guest molecule inside the cage, which enabled us to study host-guest non-covalent interactions.

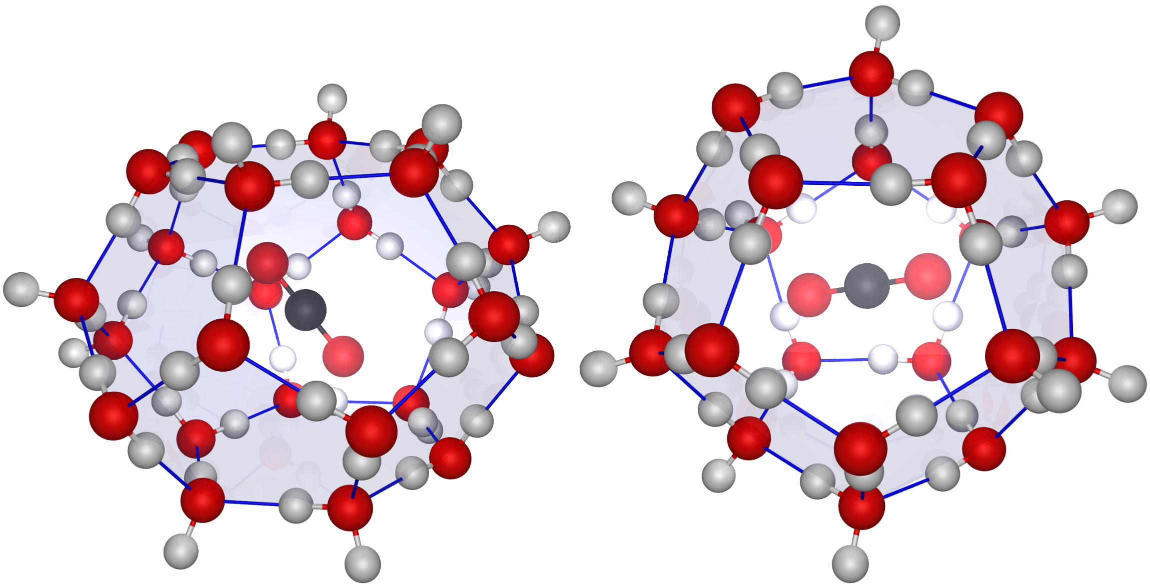

(a) H cage

(b) P cage

Figure 2.4: Example of cluster cages with CO_2

2.2.2 Periodic systems

Periodic infinite systems (such as perfect solids) can be modeled by assuming a periodic Hamiltonian, the so-called "periodic boundary conditions" (PBC). Bloch studied the solutions of the Schrodinger equation under PBC in 1928, formulating Bloch's theorem (that states that reciprocal space vectors are "good quantum numbers" for the description of one-electron wavefunctions), and enabling the calculation of the electronic structure in solids.

The code we used for periodic calculations in this work is `Quantum Espresso`[49]. It works within the plane waves/pseudopotentials approximation. Plane waves are periodic by definition, so they are very well adapted to the periodic boundary conditions. These functions have a very well defined momentum but are totally delocalized through the space, so in the cases were electrons are highly localized (as in the core) a very large amount of plane waves is necessary to describe appropriately this behaviour. Ideally, the expansion takes infinite plane waves but, under the approximation that plane waves with high kinetic energy are negligible, we define a cutoff energy to the expansion.This cutoff energy defines in practice the size of our basis set. The problem of the density at the core is avoided assuming that the core electrons are confined within a radius and they do not affect the valence electrons (the frozen core approximation). Under this assumption, it is possible to model the core electrons as a pseudopotential and perform the calculations only with the valence electrons. In this way, the computational cost is greatly reduced because there are much less electrons to simulate and they can be described by a smaller amount of plane waves. In addition, the use of plane waves allows the use of Fast Fourier Transform (FFT) algorithms to make the integration over the reciprocal space faster.

The construction of the pseudopotential, which involves several parameters (see Figure 2.5), is critically important. Good pseudopotentials should be "transferable", that is, they should model the physics of the system in different chemical environments.

The first pseudopotentials developed were the so called norm-conserving pseudopontentials (in which the pseudo-wavefunction integrates to the same number of electrons that it represents), but these pseudopotentials needed a very large number of plane waves to correctly describe the system, particularly for the more electronegative atoms. An improvement was made by Vanderbilt with the use of ultrasoft pseudopotentials, in which the norm is not conserved but the increased softness of the pseudo-wavefunction allows to reduce the number of plane waves

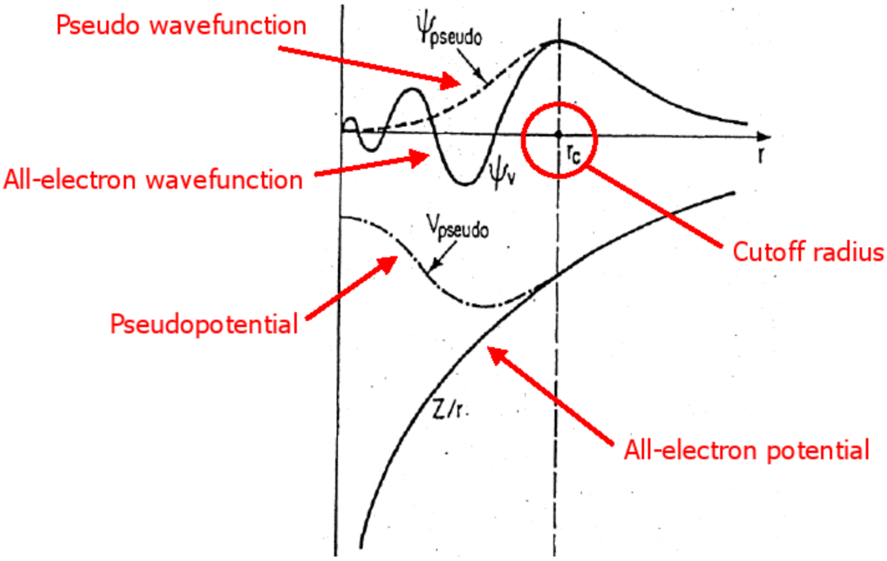

Figure 2.5: Comparison of a pseudopotential with a real potential and its wavefunctions

needed. Another improved pseudopotentials are the so-called Plane Augmented Wave (PAW) method. With these pseudopotentials the pseudo-wavefunction is related to the real wavefunction by a linear transformation. This leads to a reduced cutoff radius (that increases transferability) and they allow to reconstruct the exact wavefunction, though they need slightly larger cutoff energies than the ultrasoft pseudopotentials.

In this work we have used PAW pseudopotentials for all the atoms. The exchange-correlation functional was PW86PBE (Perdew-Wang 86 exchange plus Perdew-Burke-Ernzerhof correlation), and the dispersion interactions were accounted for by the XDM model (see subsection 2.2.1 above, and references therein). In a recent study, it is shown that this election works quiet well for non-equilibrium geometries [50]. The XDM parameters used were obtained from [17]: $a1$=0.136 and $a2$=3.178 Å. The plane waves energy cutoff was selected to 60 Ry (checking that the total energy is converged at that value) and the reciprocal space was divided into a Monkhorst-Pack [51] grid of 2$\times$2$\times$2 points. The convergence threshold for the SCF procedure is set to 10^{-8} Ry. The optimization of geometry was performed using the Broyden-Fletcher-Goldfarb-Shanno (BFGS) [52] algorithm included in the suite, relaxing the lattice parameters and all the crystallographic positions.

2.3 Non-Covalent Interactions

The so called Non-Covalent Interactions (NCI) [53, 54, 55, 56] are of critical importance in many systems, as molecular crystals and proteins. There have been different approaches to characterize these interactions, for example using distances, Quantum Theory of Atoms in Molecules [57, 58, 59] or the ELF function [60, 61]. In this work we use the properties of the reduced density gradient, s, defined as [62]:

$$s = C\frac{|\nabla\rho|}{\rho^{4/3}} \ , \ C = \frac{1}{2(3\pi^2)^{1/3}}. \tag{2.5}$$

The properties of this function highlight interactions in the low s, low density range.

NCIs also involve critical points in the electron density between the interacting system. That leads to a quick decrease of the gradient of the density to 0 at low density values. If we plot the function s *vs* the density we can see a peak in the region of low density and low density gradient, as we can see in Figure 2.6.

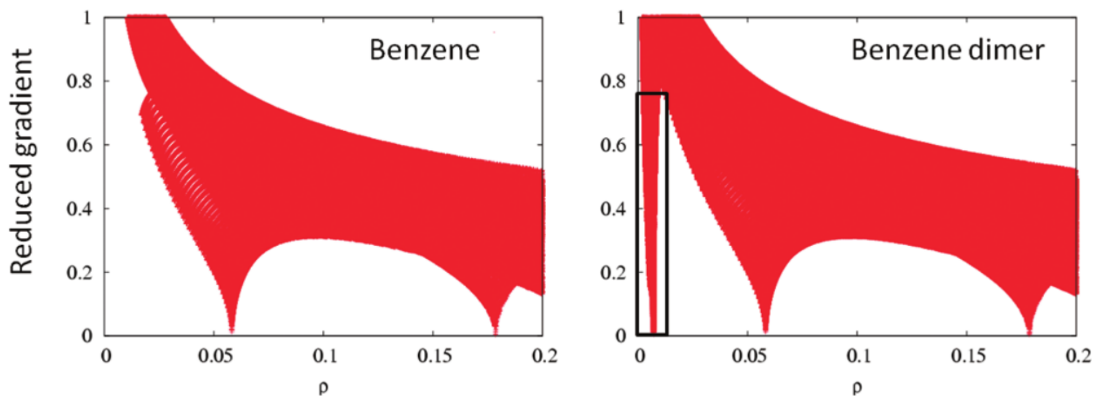

Figure 2.6: Plots of s vs ρ of the monomer and the dimer of benzene

In the absence of NCI the s *vs* ρ plot has the shape of $\rho^{-1/3}$ and thus, as we approach to $\rho = 0$ the function tends to diverge but, if we encounter a critical point the gradient becomes zero. So s becomes zero obtaining a peak at low densities.

The value of the density gives us the strength of the interaction, but a filtering criteria is necessary to classify the attractions as attractive or repulsive. This is accomplished using the properties of the Laplacian ($\nabla^2\rho$). The sign of the Laplacian tells us if the electron density tends to enter (negative) or leave (positive) a region [63].

The Laplacian can be expressed as the sum of the three eigenvalues of the Hessian, so

$$\nabla^2\rho = \lambda_1 + \lambda_2 + \lambda_3\ ,\ \lambda_1 \leq \lambda_2 \leq \lambda_3. \tag{2.6}$$

At the nuclei these three values are negative. When we are in the internuclear region $\lambda_3 > 0$. The second eigenvalue can be positive or negative. In the case of attractive interactions there will be an accumulation of charge in the intermolecular region so $\lambda_2 < 0$ and just the opposite in case of repulsive interactions (as steric clashes). So, we can make the representations of s vs $sign(\lambda_2)\rho$ and screen the different interactions appropriately. Hydrogen bonds will be at higher densities and negative values, steric clashes will be at higher densities and positive values and dispersion interactions will be around zero value. To help the interpretation it is possible to make representations of the s function at different isovalues coloring the surface accordingly to the value of $sign(\lambda_2)\rho$. A good example is the phenol dimer in Figure 2.7 where we can see the three types of interactions. As we can see, there is a hydrogen bond, depicted as a blue circle, at a density of around 0.25 with negative value of the second eigenvalue of the Hessian. At 0.2 we can see an steric clash, which is the center of the rings in reddish. And finally, at around zero, we can see the peaks of the green surface of dispersion interaction.

In this work the NCI are studied using the wavefunctions from both the periodic and cluster models. We made use of the `NCIPLOT` program [64] for clusters and `CRITIC2` program [65] for solids. Below we can see an example of input of `NCIPLOT` program with the options most widely used.

```
1               !number of wfn or xyz input files for NCIPLOT
ch4.wfn         !wfn or xyz input file
INCREMENTS 0.1 0.1 0.1 !x y z step size for the cube files
CUTOFFS 0.2 2.0 !rho and RDG cutoffs for 2d representation
CUTPLOT 0.2 0.5 !rho and RDG cutoffs for vmd 3d representation
```

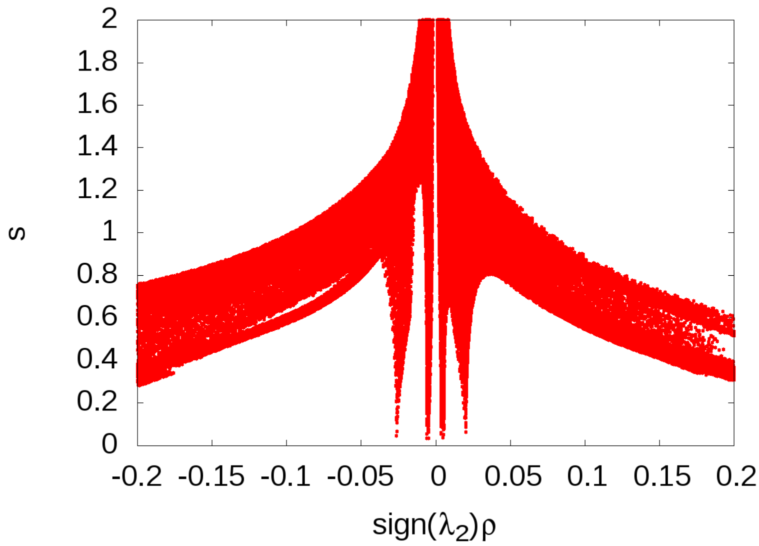

(a) s vs $sign(\lambda_2)\rho$

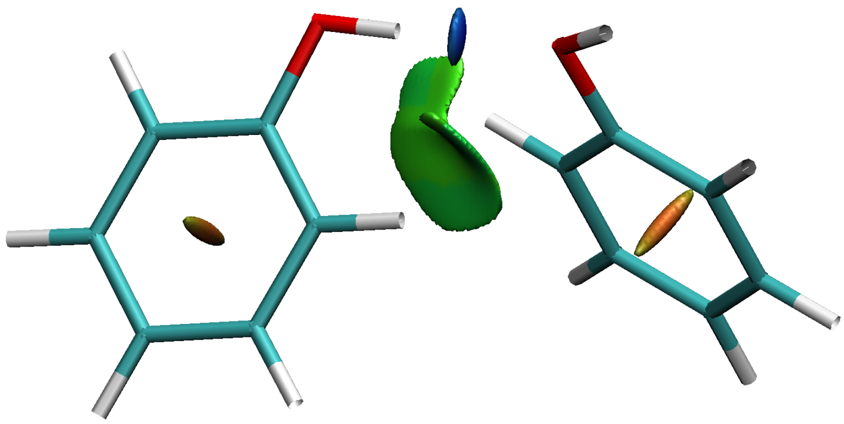

(b) Plot of isovalue 0.5 of s, blue are negative values and red are positive

Figure 2.7: NCI in phenol dimer

The options are explained as comments in the input. A wfn file is a wavefunction file in AIMPACK format, while an xyz file is a file with the coordinates of the system. In the first case the calculated density will be used while in the second case a promolecular density, from atomic ones, will be constructed. This option is useful for very big systems that make too costly to obtain an *ab initio* wavefunction.

Below we can see an input example of CRITIC2. The NCI environment has the same keywords as the NCIPLOT program.

```
crystal rho.cube    !read the structure
load rho.cube       !read the volumetric information


nciplot             !perform nci calculation
 oname 0GPa         !output name prefix
 nstep 200 200 200  !x y z number of steps for the cube files
 cutplot 0.2 1      !same as NCIPLOT
 molmotif           !draw whole molecules
endnciplot          !end of nci environment
```

The output of the calculations are a dat file with (ρ, s) pairs of data, usually plotted with GNUplot, two cube files with the information of the s function and the $sign(\lambda_2)\rho$ function (called grad and dens respectively) and a vmd file that contains a VMD script to do a quick plot of the surfaces.

2.4 Equation of State

In nature, the behaviour of all macroscopic systems is determined by thermodynamics. Under hydrostatic conditions and invariant pressure and temperature the thermodynamic function that determines stability is the Gibbs free energy:

$$G(P,T;\mathbf{x}) = E(V,S;\mathbf{x}) + PV(\mathbf{x}) - TS(V,T;\mathbf{x}) = A(V,T;\mathbf{x}) + PV(\mathbf{x}), \quad (2.7)$$

where E is the internal energy, P the pressure of the system, V the volume of the system, T the absolute temperature, S the entropy, A the Helmhotz free energy and $\mathbf{x}$ contains the geometrical parameters of the system.

Under the static approach, we consider the system at T=0 K and neglect the vibrational Zero Point Energy. Taking this into account the previous equation becomes:

$$H(P;\mathbf{x}) = E(V;\mathbf{x}) + PV(\mathbf{x}), \quad (2.8)$$

where H is the enthalpy, that now becomes the thermodynamical potential. We can also relate the (E,V) pairs with the pressure via:

$$\left(\frac{\partial E}{\partial V}\right)_{T=0} = -P, \tag{2.9}$$

which is obtained by deriving 2.8 with respect to V. The above equation allows us to define the static Equation Of State (EOS). It is possible to do the derivation including the temperature obtaining in that case: $\left(\frac{\partial A}{\partial V}\right)_T = -P$ and, thus, a relation $f(P,V,T) = 0$. Making further derivations it is possible to define the bulk modulus as:

$$B = -V\left(\frac{\partial P}{\partial V}\right)_T, \tag{2.10}$$

which is a measure of the strength of the solid. The higher the value the less compressible the material is.

There are a number of analytical EOS in solids: Murnaghan, Birch-Murnaghan (order n), Vinet or Poirier-Tarantola (see [66, 67, 68]). Numerical EOS can also be obtained. A standard procedure consists in computing the energy of the system at several volumes (relaxing the internal atomic coordinates) obtaining (E,V) pairs that can be described using one of the equation of states previously mentioned.

In this work, we studied the static equations of state of the empty, fully-CO_2-occupied, and fully-CH_4-occupied clathrates. To do this, we examined a volume grid for those three systems spanning a pressure range up to about 5 GPa, well beyond the stability range of this low pressure phase. The geometry relaxations under pressure follow the same scheme as described above, except that the calculations were done at a fixed volume. All the fitting and pressure studies were carried out with the `GIBBS2` code.[66, 67, 68]

2.5 Vibrations

The analysis of the normal modes of the system allows us to obtain the frequencies for vibrational spectroscopy studies, the main reference about molecular vibrations is the book of Wilson, Decius and Cross [69].

The procedure starts with the evaluation of the Hessian matrix. This force matrix has a $3N \times 3N$ dimension for an N dimension molecular system. Its elements are defined as:

$$f_{ij}^{cart} = \left(\frac{\partial^2 E}{\partial \xi_i \partial \xi_j}\right)_0 \tag{2.11}$$

where ξ_i is the displacement in Cartesian coordinates of each atom. The 0 subindex indicates that the derivatives are calculated at the equilibrium geometry where the energy is a minimum and thus, the first derivative is 0.

After the calculation of f^{cart} the code proceeds to its conversion to MWC, Mass-Weighted Coordinates:

$$f_{ij}^{MWC} = \frac{f_{ij}^{cart}}{\sqrt{M_i M_j}} = \left(\frac{\partial^2 E}{\partial q_i \partial q_j}\right)_0 . \tag{2.12}$$

This matrix is diagonalized obtaining $3N$ eigenvalues. Its square roots are the fundamental frequencies of the molecule, including translation and rotation, that should have values closer to 0. In `Gaussian09` the imaginary frequencies is depicted as negative frequencies. That tells us that the molecule is not in a minima.

The next step that is performed is to determine the principal axes of inertia. The origin is displaced to the center of masses (cm) using the equation $R_{cm} = \frac{\sum_\alpha M_\alpha R_\alpha}{\sum_\alpha M_\alpha}$ to calculate the position of the cm and displacing the origin using $R'_\alpha = R_\alpha - R_{cm}$. After that, the tensor of inertia is obtained

$$I_{ij} = \sum_\alpha M_\alpha \left(\delta_{ij}\left(\sum_{k=1}^{3} x_{\alpha,k}^2\right) - x_{\alpha,i} x_{\alpha,j}\right) \tag{2.13}$$

where $x_{\alpha,k}$ is the α atom coordinate and k varies between 1 and 3 being $x_1 = x$, $x_2 = y$ y $x_3 = z$. The tensor is diagonalized obtaining, thus, the principal axis of inertia and the X eigenvectors matrix.

Next, the rotational and translational coordinates are separated in order to obtain the vibrational coordinates. The translation vectors are obtained with the next equations:

$$D_1 = (\sqrt{M_\alpha}, 0, 0, \sqrt{M_\beta}, 0, 0, \ldots), \tag{2.14}$$

$$D_2 = (0, \sqrt{M_\alpha}, 0, 0, \sqrt{M_\beta}, 0, \ldots), \tag{2.15}$$

$$D_3 = (0, 0, \sqrt{M_\alpha}, 0, 0, \sqrt{M_\beta}, \ldots), \tag{2.16}$$

and rotations are calculated with:

$$D_{4i,\alpha} = ((P_y)_\alpha X_{i,3} - (P_z)_\alpha X_{i,2})/\sqrt{M_\alpha}, \tag{2.17}$$

$$D_{5i,\alpha} = ((P_z)_\alpha X_{i,1} - (P_x)_\alpha X_{i,3})/\sqrt{M_\alpha}, \tag{2.18}$$

$$D_{6i,\alpha} = ((P_x)_\alpha X_{i,2} - (P_y)_\alpha X_{i,1})/\sqrt{M_\alpha}, \tag{2.19}$$

where $i = x, y, z$, α is the atom index and P is the scalar product between the coordinates of the atom with respect to the cm (R'_α) and the corresponding row of X, the matrix that diagonalizes the tensor of inertia.

When normalizing the vectors, if the scalar product of the vector with itself is close to 0, the vector is neglected because it is not a normal mode. After normalizing the matrix D is obtained, this matrix transforms from MWC to internal coordinates. The Hessian suffers the next transformation:

$$f^{int} = D^\dagger f^{MWC} D, \tag{2.20}$$

that uses the $3N$ coordinates. The submatrix corresponding with the normal modes is then diagonalized. The eigenvectors are the columns of the L matrix and the eigenvectors are λ_i, which form the diagonal matrix Λ ($L^\dagger f^{int} L = \Lambda$).

To obtain the frequencies the relation $\lambda_i = 4\pi^2\nu_i^2$ is used. Using atomic units, the frequencies expressed as wavenumbers are:

$$\omega_i = \sqrt{\frac{\lambda_i}{4\pi^2 c^2}} \tag{2.21}$$

where c is the speed of light.

Overall is possible to see that the whole procedure involves the next transformations:

$$\Lambda = L^\dagger f^{int} L = L^\dagger D^\dagger f^{MWC} D L = L^\dagger D^\dagger M^\dagger f^{cart} M D L = l^{cart\dagger} f^{cart} l^{cart}, \tag{2.22}$$

where M is the diagonal matrix with the $1/\sqrt{M_\alpha}$ values and the l^{cart} column vectors are the normal modes expressed in Cartesian coordinates. These Cartesian coordinates are then normalized

$$\mathsf{N}_i = \sqrt{\left(\sum_\alpha^{3N} (l^{cart}_{\alpha,i})^2\right)^{-1}} = \sqrt{\mu_i} \tag{2.23}$$

where μ_i is the reduced mass of the normal mode. It is worth to note that this value is different from $1/\mu = \sum_\alpha^{3N} 1/M_\alpha$, which does not take into account the symmetry of the system. That in the previous model is included, and obtains consistent results for polyatomic molecules.

In this work we present a preliminary vibrational analysis using cluster models within the `Gaussian09` framework in the harmonic approach. The cluster consisting of a H and a P cage sharing a pentagonal face was used to calculate the vibrational modes of CH_4@sI and CO_2@sI (see Figure 2.8). We plan to carry out more computationally demanding calculations of phonons at the gamma point in the future.

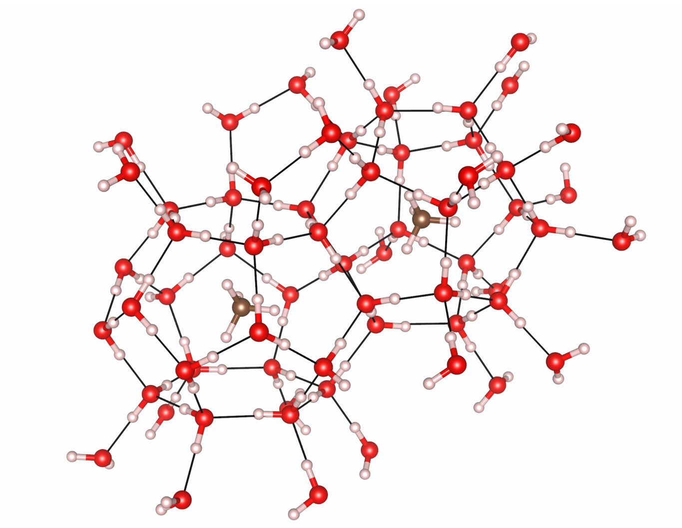

Figure 2.8: Cluster used for the calculation of vibrational modes of CH_4@sI

CHAPTER 3

RESULTS

In this chapter we present and discuss results obtained using the methodology explained in the previous chapter. We divide the presentation in four sections. The first one deals with the equilibrium structure of the unit cell (lattice parameters and internal coordinates), the study of the energetics of the internal orientation of the guest gas molecule inside the host, and the energetics of the saturation process of gas molecules inside the clathrate cavities. These results are obtained at atmospheric pressure. In the second section we present pressure effects on the geometrical parameters of the unit cell, including a comparative analysis of changes in the occupied cavities by methane and carbon dioxide. The third section analyses the effect of the NCIs on the behaviour and stability of the system, and in the fourth section we introduce preliminary results from our study on frequencies of guest and host vibrational modes.

3.1 Structure

The unit cell of the structure has been described in the previous section. There is a number of experimental studies about the CH_4@sI clathrate, while references to CO_2@sI are scarce. The experimental lattice parameter is a = 11.964 Å (280 K) [7] and 11.877 Å (123 K) [70] for methane clathrates.

Parameter	empty	$CO_2@sI$	$CH_4@sI$
a (Å)	11.665	11.540	11.646
b (Å)	11.650	11.812	11.657
c (Å)	11.646	11.579	11.633
α	89.90	88.87	89.87
β	89.83	89.86	89.83
γ	89.92	91.11	89.94
Volume (Å^3)	1582.72	1577.77	1579.32

Table 3.1: Cell parameters for empty, $CO_2@sI$ and $CH_4@sI$ hydrates

We have carried out two different geometrical optimizations of the unit cell in the three systems: empty, $CH_4@sI$ and $CO_2@sI$. Notice that all the cavities are occupied with the guest molecule in both types of optimizations. In the first one, all the degrees of freedom are relaxed without any restriction using the triclinic space group $P1$. These calculations are very expensive in terms of computational time and provide us with the equilibrium geometry of the three clathrate systems at zero pressure. In Table 3.1, we collect the lattice and angle parameters of the unit cell obtained from these calculations, while in the tables of the Appendix A we give the positions inside the cell for all the atoms of water molecules in each structure.

The average lattice parameter does not deviate noticeably from the specific a, b and c values for each structure, being the largest deviation 0.167 Å in the higher anisotropic $CO_2@sI$ system. In all cases the lattice angles are very close to 90 degrees.

In the second type of calculations, we carried out optimizations of the atomic positions at different volumes assuming a cubic unit cell. These results will be discussed later regarding pressure effects. Here we show the zero pressure lattice parameter and equilibrium volume (in brackets) from these calculations for the empty, $CH_4@sI$ and $CO_2@sI$ clathrates, respectively: 11.673 Å (1590.55 Å^3), 11.651 Å (1581.57Å^3) and 11.663 Å (1586.47 Å^3). We omit the optimized oxygen and hydrogen atomic coordinates that show very similar values to the ones from the fully relaxed-type calculations. From these results we conclude that the cubic restriction is a reasonable option to simulate the hydrate systems.

As regards the comparison with the available experimental data (only in $CH_4@sI$), our calculated values are in good agreement with the lattice parameter, considering that the effect of the temperature is to increase the lattice parameter. Furthermore, the crystallographic positions of the oxygens do not vary noticeably from the experimental ones, being most of the differences around 0.005 (crystallographic coordinates) or less. It is also to be noted that these internal coordinates remain with similar values in the empty and $CO_2@sI$ clathrates. The carbon atoms of the guest lay in the center of each cage.

It is also interesting to point out that the cell parameters in the three systems are very close between them, being slightly larger in the empty clathrate. It seems that the net effect on the structure of the guest is not too important.

In Table 3.2 we collect the most relevant average distances in the empty and gas filled gas clathrates: intra-molecular and intermolecular water distances ($d_{\mathrm{OH}}^{\mathrm{intra}}$, $d_{\mathrm{OH}}^{\mathrm{inter}}$, $d_{\mathrm{OO}}^{\mathrm{inter}}$), and the average guest-host (oxygen) distances from the center of the P ($d_{\mathrm{GH_P}}$) and H ($d_{\mathrm{GH_H}}$) cages. All the values come from the fully relaxed-type calculations.

Hydrate	$d_{\mathrm{OH}}^{\mathrm{intra}}$	$d_{\mathrm{OH}}^{\mathrm{inter}}$	$d_{\mathrm{OO}}^{\mathrm{inter}}$	$d_{\mathrm{GH_P}}$	$d_{\mathrm{GH_H}}$
$CH_4@sI$	1.000	1.708	2.706	3.787	4.185
$CO_2@sI$	0.999	1.713	2.710	3.790	4.188
Empty	1.000	1.710	2.708	3.789	4.189

Table 3.2: Relevant distances, in Å, of $CH_4@sI$, $CO_2@sI$ and empty hydrates

As we can see the distances are barely affected by the presence of the guest, as occurs with the lattice parameter previously discussed. Our calculated $d_{\mathrm{OO}}^{\mathrm{inter}}$, which is the most relevant distance in the structure, agrees with the experimental value of $\sim$ 2.75 Å found in a number of gas hydrates sI [70]. The distance corresponding to the covalent bond, $d_{\mathrm{OH}}^{\mathrm{intra}}$, is slightly larger than in the gas water molecule, whereas $d_{\mathrm{OH}}^{\mathrm{inter}}$ lies within typical values of a hydrogen bond. Clearly, distances in the P cage are about 0.4 Å shorter than in the H cage. It is also interesting to calculate the volumes of the P and H cages in the three systems. We found similar volumes around 155 Å^3 for the P cage and around 220 Å^3 for the H cage. The experimental values in CH_4@sI are 164.1 Å^3 and 232.4 Å^3 for P and H cages respectively. Differences are due to the difference in the lattice parameter.

After detailed analysis of these data and individual interatomic distances, we can conclude that whereas methane does not affect the geometry of the empty clathrate framework, carbon dioxide produces slight distortions of the cavities with a greater effect in the P cages. The data maintains the trend previously depicted of similar values, but we remark the value of the distortion of the P cage in the case of the CO_2 hydrate that is bigger than the one observed when methane is the guest. affects more the structure of the P cage in comparison to the methane.dd

The values of the bond lengths of the guest molecules are gathered in Table 3.3, where we also illustrate the influence of encasulaption. As we can see, the bond lengths are slightly affected by the confinement, being the effect larger in the case of the P cage, due to its smaller size.

Molecule	$d_{\mathrm{CX}}^{\mathrm{P}}$	$d_{\mathrm{CX}}^{\mathrm{H}}$	$d_{\mathrm{CX}}^{\mathrm{Gas}}$
CH_4	1.091	1.093	1.094
CO_2	1.169	1.171	1.172

Table 3.3: Bond lengths (in Å) of the guest molecule

3.1.1 Guest-Host geometry optimization

To better describe the orientation of the guest molecule inside of the host, a study of the energetics of the system with different orientations of the guest molecule was performed. That was done by means of partial optimizations in which the coordinates of the guest were frozen and the rest of the unit cell was allowed to relax.

In the case of methane the difference in energy between the lowest and highest energy configurations is around 0.5 kcal/mol. That means that methane can rotate freely inside the cage an has no preference for one orientation or another. If we look at $CO_2@sI$ we encounter that the difference between the lowest and highest energy configurations is between 5 and 6 kcal/mol. In Figure 3.1 we plot a spherical representation of the energetic landscape inside the cage and the corresponding projection in a 2D map for the $CO_2@sI$

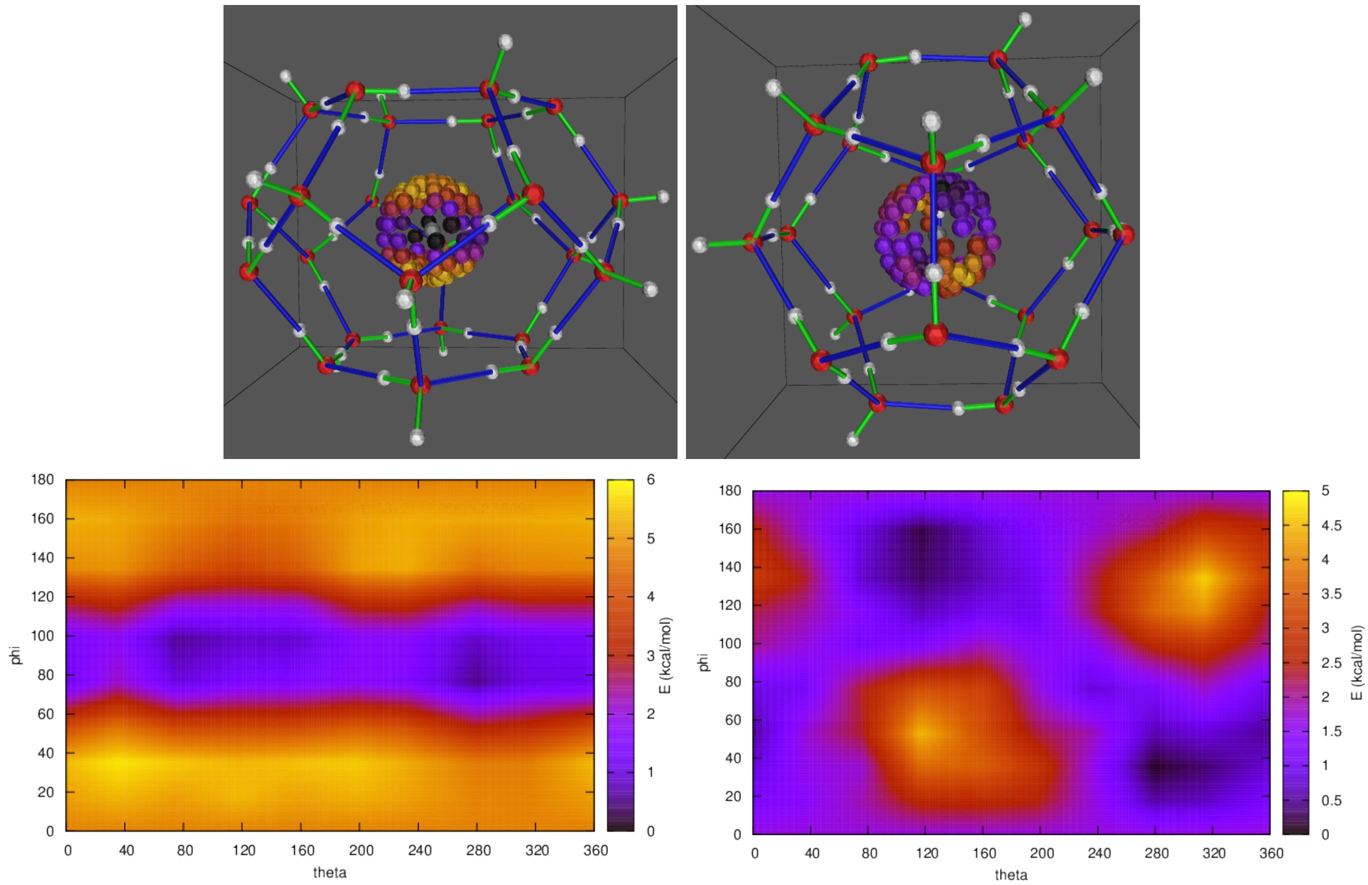

(a) H cage

(b) P cage

Figure 3.1: Energy maps analyzing different orientations of CO_2 in the cages of sI

In these maps, theta is the angle formed by the carbon dioxide molecule with the x axis, and phi is the angle formed by the molecule with the z axis. We take the z axis perpendicular to the hexagonal face of the H cell, which is also the c crystallographic axis. We maintain the same axis for the P cage. In the representations, the red balls are the oxygens, the white balls are the hydrogens, the green bars are O-H covalent bonds and the blue bars are hydrogen bonds. In the maps the lowest energy conformations are coloured in purple and the highest energy ones are coloured in yellow.

As depicted in the plots, in the H cage the most favorable orientation of carbon dioxide is found when the three atoms lie in the equatorial plane parallel to the hexagonal faces. In the pentagonal case, the most favorable orientation coincides with the situation in which carbon dioxide is perpendicular to two parallel faces of the dodecahedron. In Figure 3.2 we can see these two optimized orientations.

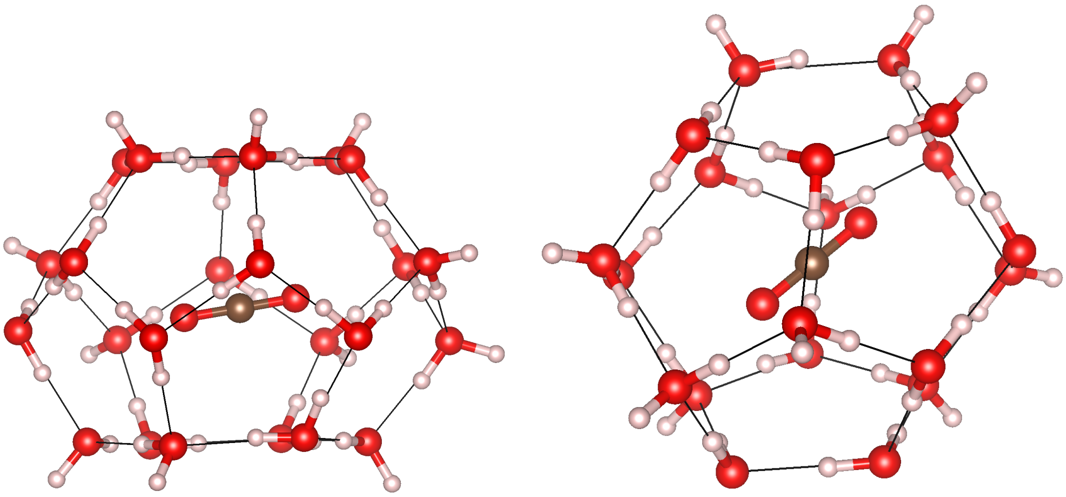

Figure 3.2: CO_2 most stable positions in H cage (left) and P cage (right)

3.1.2 Formation energy

In this section we will study the energetics involved in the saturation of all the cavities with CH_4 or CO_2 molecules. Firstly, we carry out a detailed analysis of energy contributions to the process in which only one guest molecule (G) and one cage (C) are involved: G+C $\rightarrow$ G@C. Results are presented for the case of carbon dioxide due to the fact that, as explained in the previous section, CO_2 shows bigger energy changes depending on its orientation. These calculations were performed using cluster models of 63 and 75 atoms for P and H cages, respectively.

We can assume that the deformation energy is very small because the change in distances of the guest molecule from the free molecule to the enclathrated situation is around 0.01 Å, and the cage is hardly affected by the guest, as we saw earlier. So the main component of the formation energy will be the interaction energy. In Tables 3.4 and 3.5, we summarize the calculated interaction energies without dispersion and with several dispersion corrections. The interaction contribution is calculated including BSSE corrections. D2, D3, XDM refers to the dispersion corrections described previously, and "Total" includes both the interaction and the dispersion contributions. "Stable" and "unstable" are the lowest and highest energy configurations in the geometry optimization of the previous section, respectively.

B3LYP	H stable	H unstable	P stable	P unstable
Interaction	1.61	4.46	2.98	12.22
D2	-7.30	-7.54	-10.73	-10.43
D3	-8.44	-8,20	-10.68	-10.53
XDM	-7.07	-7.34	-8.89	-8.67
Total-D2	-5.70	-3.07	-7.75	1.79
Total-D3	-6.83	-3.74	-7.70	1.70
Total-XDM	-5.46	-2.87	-5.91	3.55

Table 3.4: B3LYP energies of interaction for CO_2 clathrates

PW86PBE	H stable	H unstable	P stable	P unstable
Interaction	0.19	3.05	1.19	10.25
Grimme3	-6.47	-6.26	-7.75	-7.65
XDM	-5.33	-5.13	-5.89	-5.74
Total-G3	-6.27	-3.21	-6.56	2.60
Total-XDM	-5.13	-2.08	-4.70	4.51

Table 3.5: PW86-PBE energies of interaction for CO_2 clathrates

The first observation we can make is that dispersion contributes to stability as the most important stabilizing term. However, as the dispersion energy contributes very similarly to all the conformations, it can be concluded that it is the interaction energy term the one that determines the final orientation of the guest molecule in the cage. It is important to see that this conclusion is independent on the approach used to evaluate the dispersion energy.

In these cluster calculations we obtain the same lowest energy configuration for CO_2 in both cages. However, crystal lattice effects seem to be important because the differences between the highest and lowest energies are larger for the P cage and smaller for the H cage in the cluster calculations compared with solid calculations.

Now we present the results of the energetics of progressive occupations of P and H cages by methane and carbon dioxide molecules using the periodic approach. In each step we include one more molecule and optimize the system. The release of energy is calculated with respect to the empty clathrate and the free molecules. All the results are displayed in Figure 3.3.

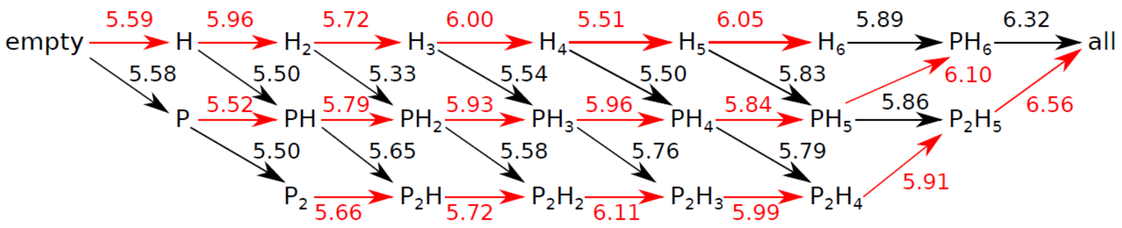

(a) CH_4

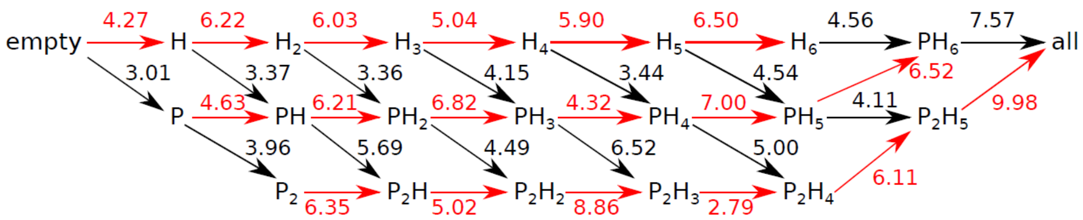

(b) CO_2

Figure 3.3: Partial occupation energies for CH_4 and CO_2 clathrates

The red lines are steps in which the cage occupied is of type H and the black lines represent the occupation of a P type cage. Over the arrow is the amount of energy released in the process (that means that the process is favorable if the number is positive). Several occupation orderings were studied and are plotted in the diagram. A general equation to explain the process at a given step is

$$P_nH_m + (l - n + k - m)G \rightarrow P_lH_k, \tag{3.1}$$

where we represent the number of P and H cages occupied by a guest molecule (G = CO_2 or CH_4) with a letter in the subindex. It is worth mentioning that $n+m \leq 8 \geq l+k$, $n \leq 2 \geq l$ and $m \leq 6 \geq k$ because there are 2 P cages and 6 H cages per unit cell.

In the case of carbon dioxide we obtain a total energy difference from empty to saturation of 46.09 kcal/mol (the eight cavities are occupied). A similar amount is obtained for methane, 47.04 kcal/mol. It is pointed out that in the case of the methane there is no preference for one cage or another, obtaining a mean energy of occupation of 5.88 kcal/mol for H cages and 5.69 kcal/mol for P cages. On the other hand, carbon dioxide shows preference for the H cages with a mean energy of occupation of 6.03 kcal/mol, while with P cages we obtain 4.56 kcal/mol. That means that, assuming perfect diffusion and guest molecule excess, the clathrate should undergo to saturation.

In Table 3.6 we collect calculated values for the formation energy from cluster and solid simulations.

Tot. Ener.	H/B3LYP	H/PW86PBE	P/B3LYP	P/PW86PBE	H/Solid	P/Solid
D2	-5.70	–	-7.75	–	–	–
D3	-6.83	-6.27	-7.70	-6.56	–	–
XDM	-5.46	-5.13	-5.91	-4.70	6.03	4.56

Table 3.6: Summary of total formation energies for CO_2@sI clathrate

Contrarily to cluster calculations, the stabilization energy in the H cage is greater than in the P cage in the solid, though the energy differences are very small. We hypothesise that the electrostatic potential created by the periodic system might be related with these energy differences.

3.2 Pressure effects

We have studied the effects of hydrostatic pressure on the structure of empty sI, $CH_4@sI$, and $CO_2@sI$ systems, and on the formation energy involved in these gas clathrate hydrates. Results are given up to 1 GPa, beyond the pressure stability range of this phase [7]. As we have indicated in the previous section, optimizations were carried out at fixed volumes using the constrain of a cubic unit cell, and allowing the atomic coordinates to relax in order to minimize the total energy.

The static equations of state (EOS) of sI, $CH_4@sI$, and $CO_2@sI$ are displayed in the volume-pressure diagrams of Fig. 3.4 (left). We have had difficulties in choosing the same fitting procedure to derive EOS parameters for the three systems. For this reason, the values we report here should be taken with caution, although we have found consistency after combining different types of evaluation. From the energy-volume computed points, we calculate pressure-volume data using numerical fittings to polynomial of different degrees. Using a fixed value for the first pressure derivative of the bulk modulus, B_0'=4, and assuming a linear dependence of the bulk modulus with pressure, B=$B_0 + B_0' \times P$, we found B_0 values of 15.7 GPa, 16.5 GPa, and 16.2 GPa for, respectively, sI, $CH_4@sI$, and $CO_2@sI$. These values follow the bulk modulus-volume inverse law: the greater the volume the lower the bulk modulus, and are also consistent with the rate the relative volume decreases with pressure, as displayed in Fig. 3.5. In Fig. 3.4(right), we show how the difference of the unit cell volumes of $CH_4@sI$, and $CO_2@sI$ with respect to sI decreases as pressure increases. This is again consistent with the lower bulk modulus calculated for the sI empty structure.

Given the fact that the cages fill up the unit cell, it is possible to carry out a partition of the crystal compressibility (κ) in terms of P and H contributions. This kind of decomposition has been proposed for atoms [71] and polyhedra [72]. Using the following definitions for the compressibility associated to the P (κ_P) and H (κ_H) cages:

$$\kappa_P = -\frac{1}{V_P}\frac{\partial V_P}{\partial P}, \quad \kappa_H = -\frac{1}{V_H}\frac{\partial V_H}{\partial P}, \tag{3.2}$$

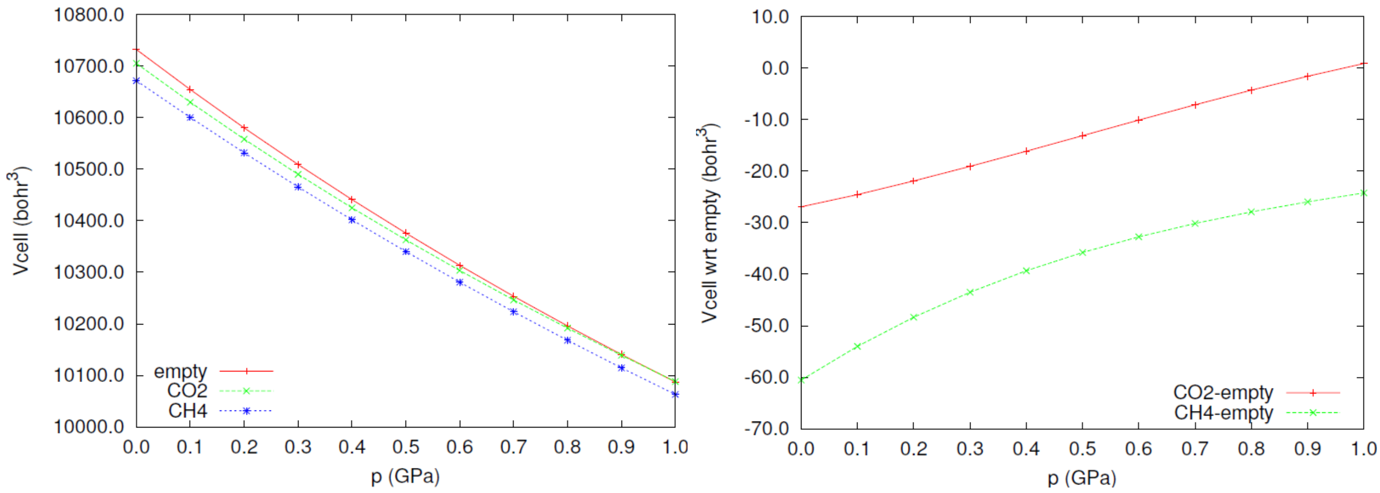

(a) EOS

(b) Volume with respect to empty

Figure 3.4: EOS curves for $CH_4@sI$, $CO_2@sI$ and empty clathrates (left) and effect of pressure on the unit cell volumes of $CH_4@sI$ and $CO_2@sI$ with respect to the empty hydrate

we can easily arrive to the expression of κ in terms of κ_P and κ_H:

$$\kappa = f_P\kappa_P + f_H\kappa_H, \tag{3.3}$$

where f_P and f_H are the relative volumes (occupation fractions) of P and H cages, respectively, in the unit cell:

$$f_P = \frac{2V_P}{V}, \quad f_H = \frac{6V_H}{V}. \tag{3.4}$$

In all these equations V_P and V_H stand for the volumes of the P and H cages, respectively.

As not all the P (or H) cages have the same volume, an accurate determination of the EOS parameters for these cages is difficult. Using average values, we have evaluated the trends that the normalized volumes of these cages exhibit as pressure is applied. The curves are represented in Fig. 3.5. What is remarkable to notice is the higher and lower compressibilities of P and H cages, respectively, compared with the unit cell in each of the system. This is a consequence of the fact that the cage with the highest compressibility is also the one with the greatest fractional occupation (more than 80%) of the unit cell. Compared with the P cage, we observe again that it is the cage with the highest volume the one that has the highest compressibility. An accurate determination of EOS parameters for these cages is in progress. These cage-EOS could be transferred to other phases (sII, sH) of CH_4 and CO_2 clathrate hydrates where these cages are also present.

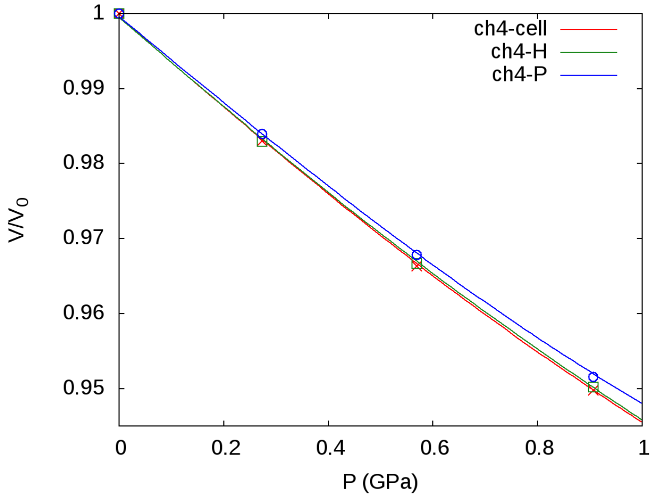

(a) CH_4@sI

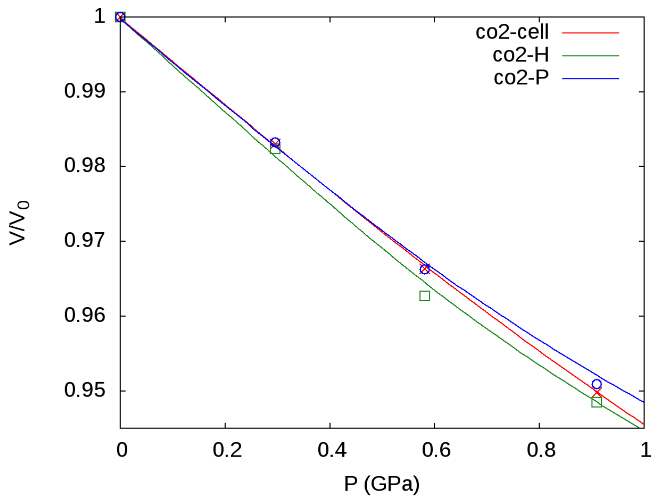

(b) CO_2@sI

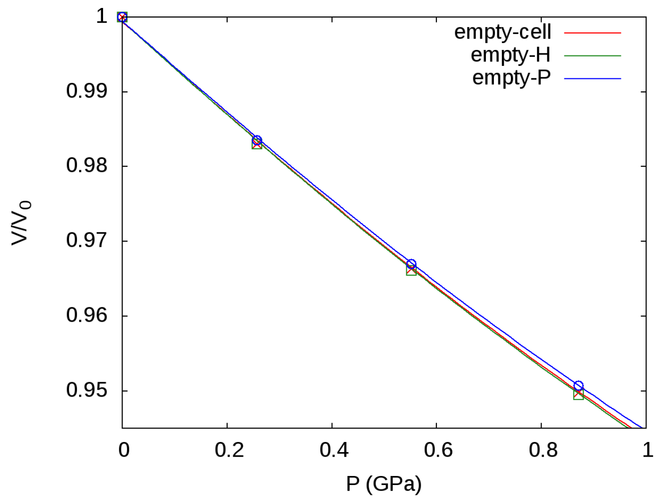

(c) Empty clathrate

Figure 3.5: Normalized volume-pressure plots for CH_4@sI, CO_2@sI and empty clathrates

To end up with pressure effects, we examine in Fig. 3.6 how the stabilization of the sI lattice induced by the occupation of CH_4 and CO_2 molecules change as pressure is applied. Average values are used. We observe that the stabilization with respect to the empty clathrate is enhanced for both guest molecules at least up to 1 GPa. Besides, the stabilization effect of CO_2 shows a greater slope than that of CH_4, though in absolute values is still lower at 1 GPa. The existence of a greater stabilizing guest-host interaction with pressure will be analyzed in the next section.

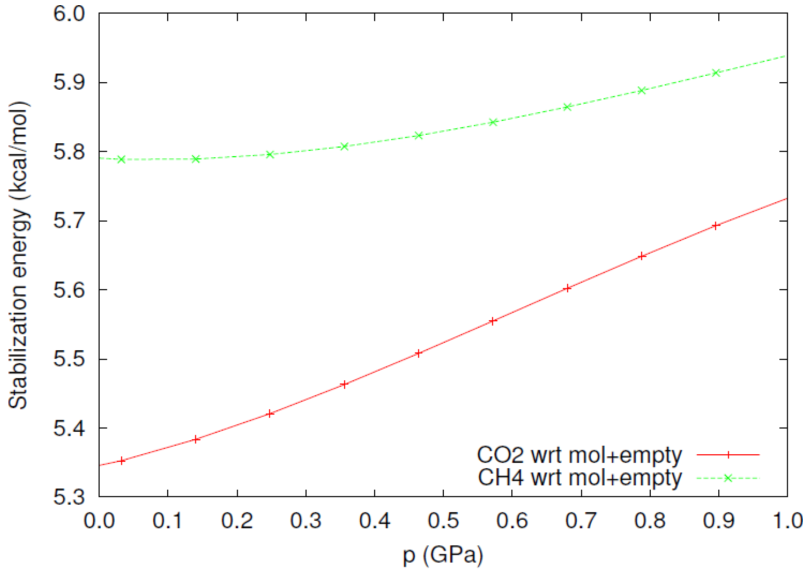

Figure 3.6: Stability with pressure

3.3 Chemical bonding. NCI

In this section we will describe non covalent interactions, which are the main type of chemical interactions in these systems. We study how these interactions are affected in each cage by pressure and orientation. Results from calculations on finite clusters and periodic systems were compared. We did not find substantial difference between them. Therefore,we can conclude that there is not any cage to cage (interactions between guest molecules of different cages) effect that NCI can detect.

In Figure 3.7 we can see the NCI surfaces at two different pressures in both types of cages of the CH_4@sI structure. The color code is blue for hydrogen bonds (attractive interaction) and green for dispersion interactions. The isosurfaces are at the 0.5 value of s and in the (-0.03,0.03) range of density, blue means

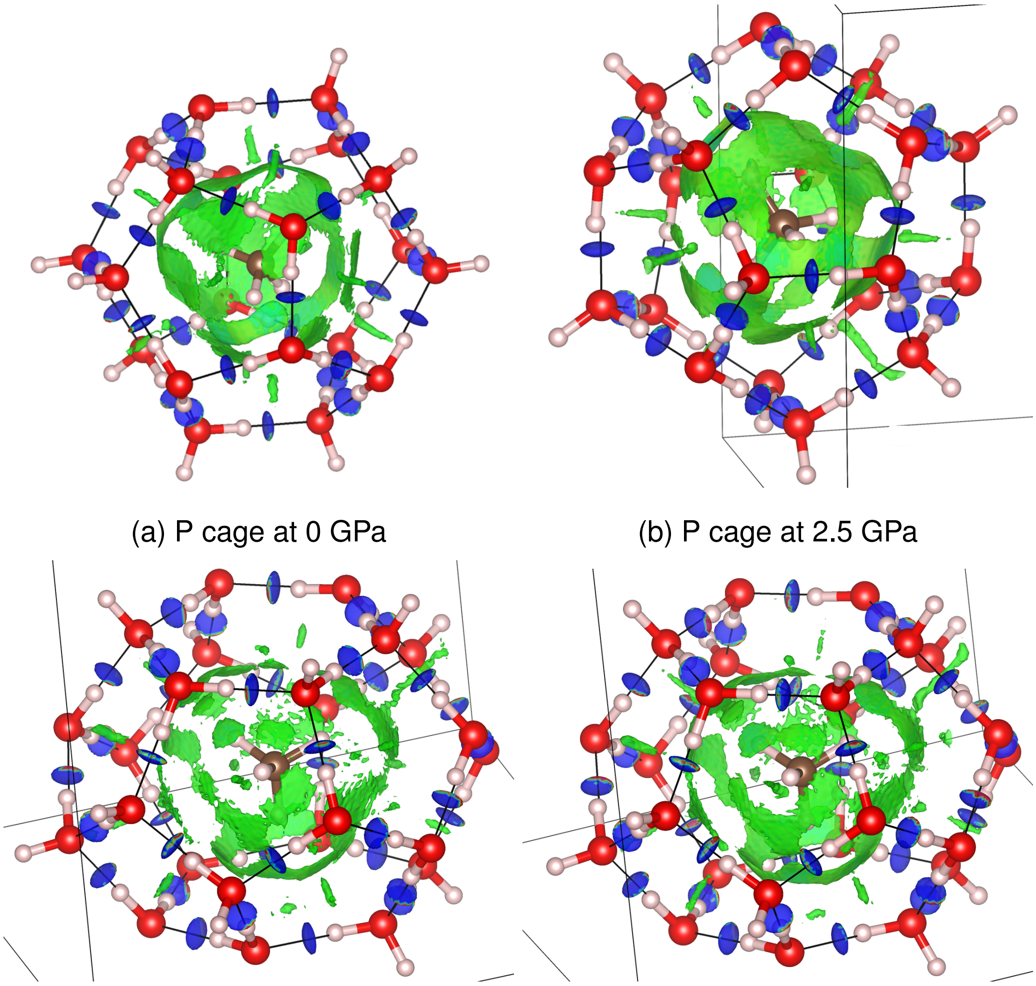

(a) P cage at 0 GPa

(b) P cage at 2.5 GPa

(c) H cage at 0 GPa

(d) H cage at 2.5 GPa

Figure 3.7: NCI plots of CH_4@sI hydrate

negative values. The first observation we can do is that, as the P cage is smaller than the H cage, the amount of dispersion interactions is bigger in the P cage than in the H cage. That agrees with the r^{-6} dependence of the dispersion with the distance (r). In recent studies it has been showed that the volume of NCI is proportional to the dispersion correction [73]. We can also see the interactions of all the water molecules between themselves through hydrogen bonding. We have not found any strong interaction between the guest and the host. The effect of pressure is to decrease the volume of the cages so we can see that the amount of dispersion interactions between the guest molecule and the cage increases because the atoms are closer to each other. There is also another pressure effect:

the strength of the hydrogen bonds are enhanced as pressure is applied. This is clearly displayed in Figure 3.8. The dispersion forces lay around 0 density and

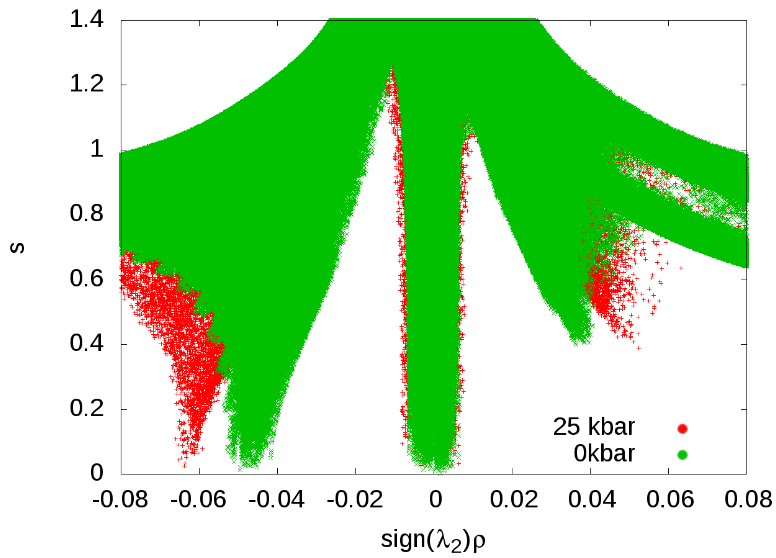

Figure 3.8: s vs ρ plot of CH_4@sI at 0 and 2.5 GPa

the hydrogen bonds around 0.05 values on the negative side. The effect of pressure is to displace the hydrogen bonds towards higher densities. The dispersion forces are very little affected by this effect. In Figure 3.9 we can see analogous results for CO_2@sI.

The trends in this case are similar to the previous $CH_4@sI$ system. We can observe that the amount of interactions between the guest and the host is bigger (there is more surface) in the P cages than in the H cages. The effect of pressure in the surfaces is less evident than in the case of methane, probably due to the different shape of the molecule, being methane more symmetric than carbon dioxide. In the Figure 3.10 we can complete the information with the effects on the hydrogen bonds and the analysis of the NCI peaks.

It is possible to see that the dispersion peaks around 0 density are wider than in the previous case. This could be related with stronger interactions between the carbon dioxide and the host. The behaviour of the hydrogen bonds is the same that in the case of methane. Though we can see that under pressure the hydrogen bonds peak become wider, meaning that there is more variation in the

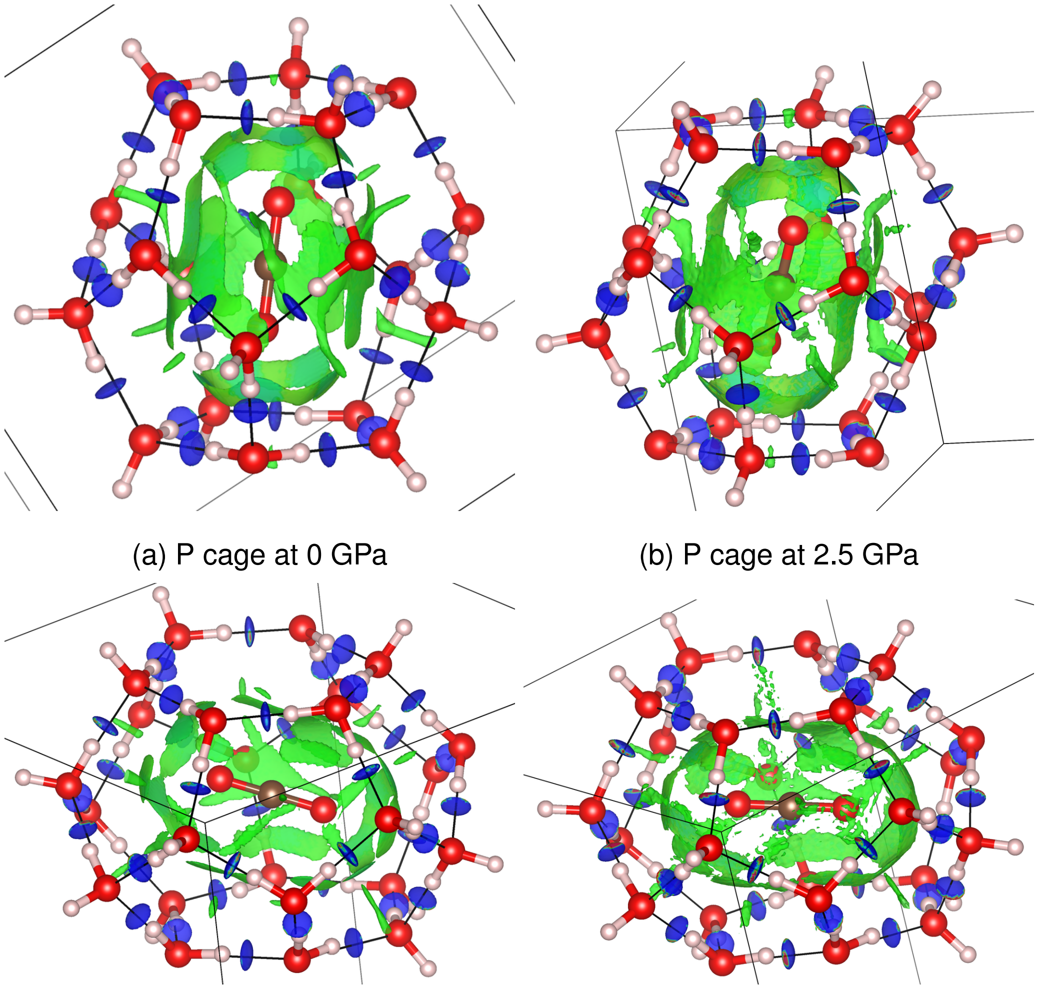

(a) P cage at 0 GPa

(b) P cage at 2.5 GPa

(c) H cage at 0 GPa

(d) H cage at 2.5 GPa

Figure 3.9: NCI plots of CO_2@sI hydrate

strength of the interactions, certainly due to the bigger distortion in the cages produced by the carbon dioxide anisotropy (it is a linear molecule, less symmetric than the methane).

Finally, we carry out a comparison between the lowest and highest energy configuration. The results are in Figure 3.11 We can see that the behaviour is similar in both cages. We find a stronger interaction in the case of the unstable conformation between the oxygen of the carbon dioxide and one oxygen of the water molecules of the cage. To try to explain which is the driving force of the final orientation of the molecule in the cage, we performed energy decomposition calculations with the code `ADF` [74]. The energy is decomposed in steric (Pauli

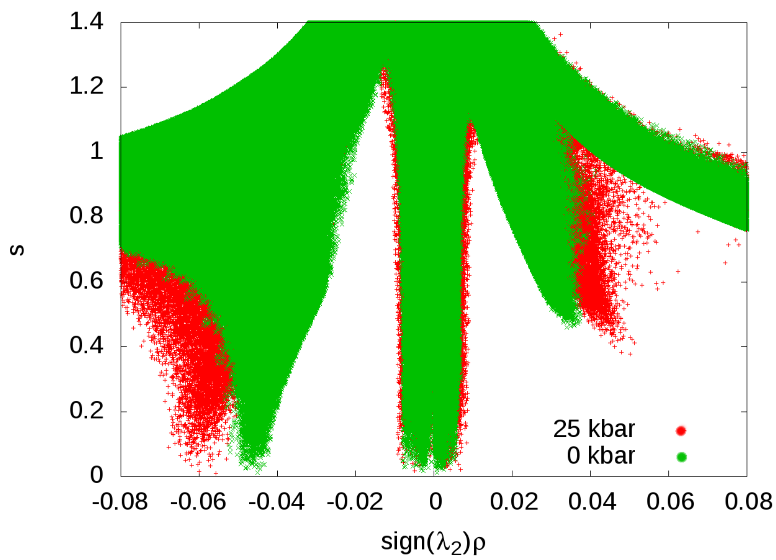

Figure 3.10: s vs ρ plot of CO_2@sI at 0 and 2.5 GPa

Type	Stable	Unstable	$Vert_1$	$Vert_2$	Hor_1	Hor_2
Steric	0.50	3.50	1.49	2.15	1.72	1.09
Orbital	-2.51	-2.68	-2.60	-2.66	-2.55	-2.60
Dispersion	-7.34	-7.04	-7.23	-7.07	.7.29	-7.29
Total	-9.35	-6.21	-8.35	-7.57	-8.12	-8.81

Table 3.7: ADF decomposition energy(kcal/mol) for H cage of CO_2@sI

repulsion + electrostatic interactions), orbital (charge transfer + polarization) and Grimmes's D3 dispersion correction contributions. We took four additional orientations with energies in the middle of the two previous values for the case of the H cage: two varying the angle with respect to the z axis ($Vert_1$, $Vert_2$) and two with respect to the x axis(Hor_1, Hor_2). In Figure 3.12 we can see these orientations. In Table 3.7 there is a summary of our results.

Looking at these results we can see that in the case of orbital interaction and dispersion corrections contributions the values do not change very much from one to another. However, the differences in the case of the steric interactions are bigger, and correlates with the total energies. So, we can conclude that the main driving force for the final orientation of CO_2 in both cages is the steric repulsion.

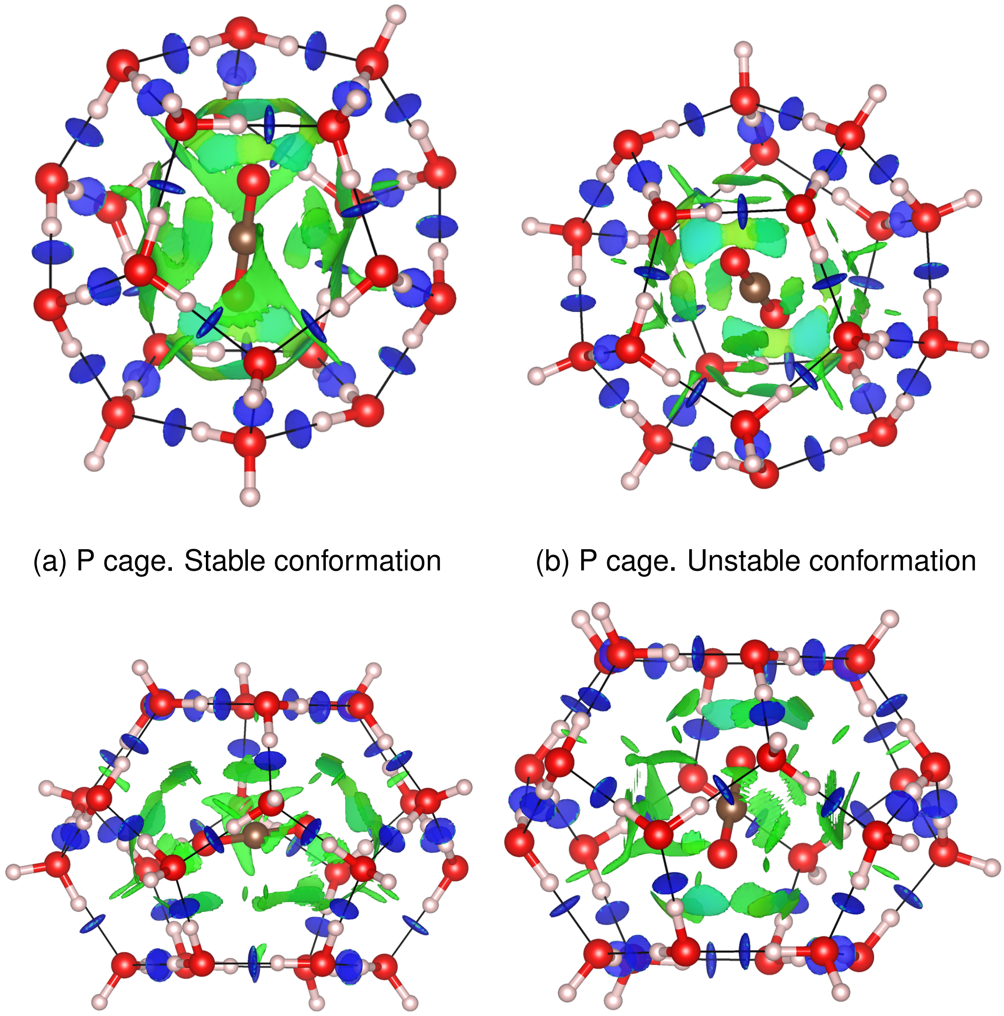

(a) P cage. Stable conformation (b) P cage. Unstable conformation

(c) H cage. Stable conformation (d) H cage. Unstable conformation

Figure 3.11: NCI plots of CO_2@sI in two orientations

3.4 Vibrations

The analysis of the vibrational modes in gas clathrates hydrates is a key issue for many reasons. Infrared and Raman frequencies and intensities provide relevant data on the local environment of the guest molecules, including the occupancy of the cages along with information on the guest-host interactions and the dynamics of the guests in the cages. If we analyze how the frequencies of the vibrational modes belonging to the host and guest atoms of the clathrate change with respect to values of water, methane and carbon dioxide, then we can obtain characteristic signatures that allow to identify the presence of these gas clathrate systems in a

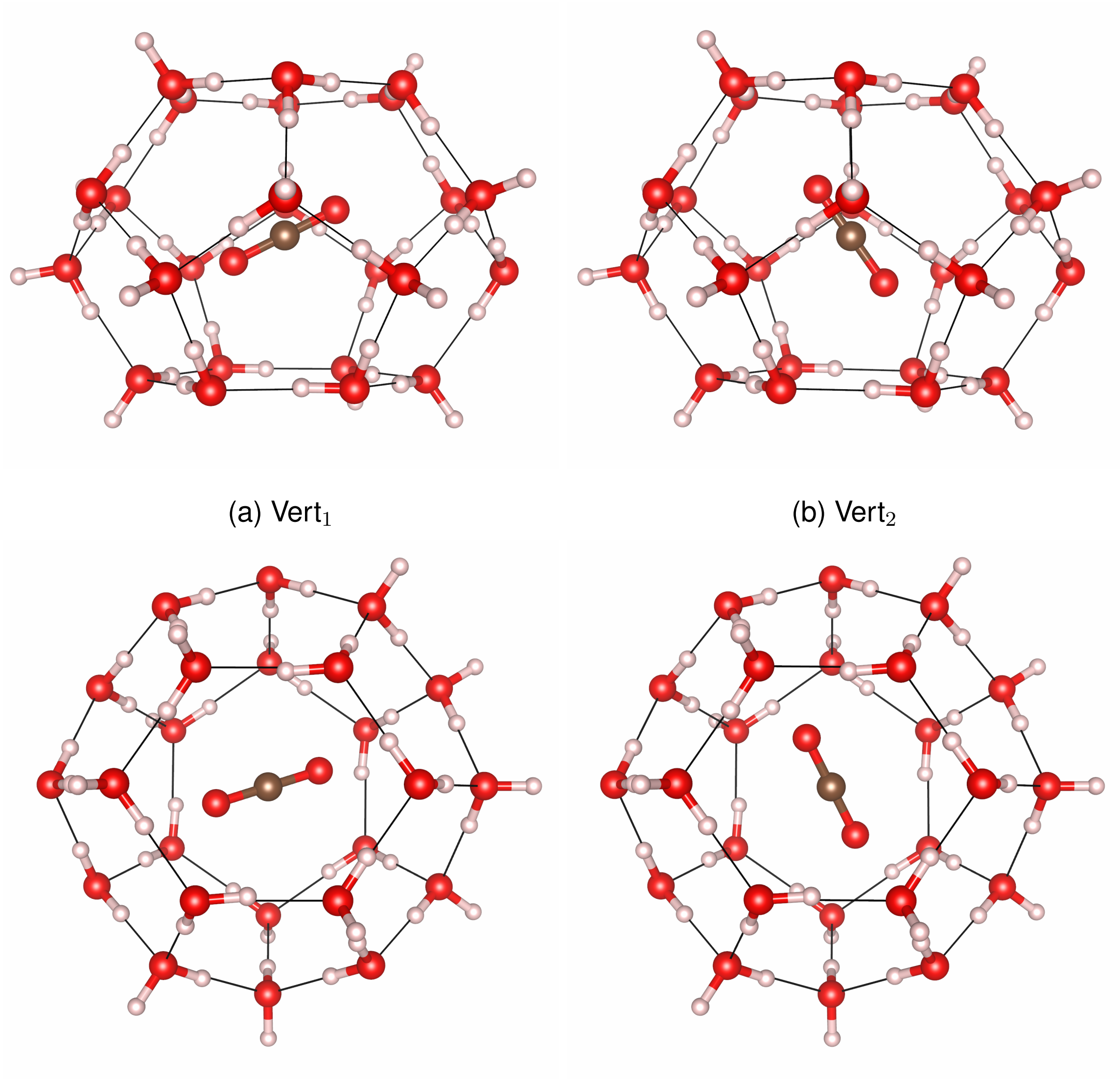

(a) Vert_1 (b) Vert_2

(c) Hor_1 (d) Hor_2

Figure 3.12: Additional orientations used in the `ADF` study

particular environment.

We have looked for previous theoretical and experimental investigations related to the analysis of the vibrational spectra in the systems studied in this Master Thesis. We have found a number of works for $CH_4@sI$ (see for example recent publications [75, 76, 77] and references therein) but no data for $CO_2@sI$. We can distinguish two types of analysis. The first one has to do with the variations of the frequencies associated with localized modes of the water and guest molecules of the clathrate with respect to the corresponding values of gas, liquid or solid phases of isolated water, methane or carbon dioxide. There is not a consensus about the shifts of the frequencies. Controversial data from previous theoretical and experimental studies inform either on a blue shift of the antisymmetric stretching (AS) C-H mode due to encasulaption [76] or a red shift of this mode of 31 cm^{-1} (calculated by Marion *et al.* [77]) and 20 cm^{-1} (experiments of Dartois and Deboffe [78]). In the case of the symmetric and antisymmetric stretching O-H modes (SS and AS) of water, Ramya *et al.* [76] found red shift upon clathrate formation in agreement with reported values of Marion *et al.* [77]). The second one is intended to distinguish changes on the frequencies due to the type of the cage occupied by the guest. The analysis is clearer here since the comparison is between data of the same system. Frequencies of both, SS and AS modes in methane, are higher in the P cage than in the H cage, and this blue shift is higher for the AS mode [75].

Our results come from cluster calculations using a cluster model consisting of the two cages sharing a pentagonal face (see Figure 2.8). As we present here preliminary results from our calculations, the analysis will be limited to the most important modes of water and the guest molecules. For water, we discuss the stretching and bending modes, whereas for methane and carbon dioxide we analyze stretching modes.

We performed *in vacuo* geometry optimizations of methane, carbon dioxide and water obtaining their frequencies at the same level of theory as the cluster calculations. We obtain the following values. For methane, 3044 cm^{-1} for the SS and 3067 cm^{-1} for the AS modes. For carbon dioxide, 1282 cm^{-1} for SS and 2283 cm^{-1} for AS modes, and for water molecules, 1619 cm^{-1} for the Bending (B_{H_2O}), 3618 cm^{-1} for SS and 3783 cm^{-1} for AS. These values are in good agreement with well known theoretical and experimental data.

In Tables 3.8, 3.9 and 3.10, we present frequencies of the previously relevant normal modes. As the symmetry is lost in the cluster, we average the values of the originally degenerated components. For water modes there are many contributions, so we give the values of the lower and higher frequencies in the band. As the stretching vibrations of water are very difficult to classify into symmetric and antisymmetric stretching the values of the band will be classified as Stretching (S_{H_2O}). Cage dependencies are also studied, so we include a H or P subindex (for H and P cages, respectively) into the molecule normal mode nomenclature.

P (GPa)	SS_P	SS_H	AS_P	AS_H	B_{H_2O}	S_{H_2O}
0.009	3069	3050	3194	3140	1680–1809	3059–3504
0.282	3070	3050	3194	3173	1681–1812	3022–3492
0.578	3074	3051	3200	3174	1681–1818	2997–3480
0.915	3077	3052	3204	3177	1683–1819	2970–3467

Table 3.8: Relevant vibrational frequencies, in cm^{-1}, of CH_4@sI clathrate

P (GPa)	SS_P	SS_H	AS_P	AS_H	B_{H_2O}	S_{H_2O}
0.036	1368	1358	2433	2422	1674–1818	3053–3513
0.332	1370	1358	2438	2421	1678–1820	3038–3509
0.617	1369	1358	2436	2421	1675–1823	3001–3499
0.946	1370	1360	2437	2424	1670–1827	2981–3486

Table 3.9: Relevant vibrational frequencies, in cm^{-1}, of CO_2@sI clathrate

P (GPa)	B_{H_2O}	S_{H_2O}
0.101	1679–1812	3069–3501
0.358	1679–1815	3043–3489
0.653	1679–1818	3015–3477
0.972	1680–1821	2986–3464

Table 3.10: Bending and stretching frequencies of water in empty clathrate

As we can see, the enclathration effect produces a blue shift in the guest molecule frequencies. This effect is much clearer in the case of carbon dioxide, which changes from 1282 to around 1360 cm^{-1}, than in methane, changes are from 3044 to around 3060 cm^{-1}. The size of the cage also plays a role in the shift as the smaller P cage induces larger shifts than the H cage. The influence of pressure is not very important in the guest molecule stretching modes. With respect to the water molecules, we can see that the modes are independent from the guest: we obtain very similar values in the three systems. The pressure has not any effect on the bending modes. However, the stretching modes are redshifted around 80 cm^{-1} as the pressure increases up to 1 GPa. The effect is the same in the three systems (CO_2@sI, CH_4@sI and empty clathrates) at different pressures.

In Figure 3.13, 3.14 and 3.15, we collect the calculated spectra for the cluster systems (CO_2@sI, CH_4@sI and empty clathrate).

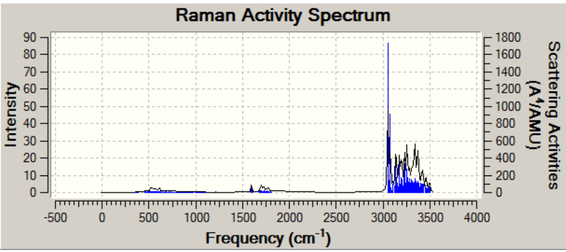

(a) 0.009 GPa

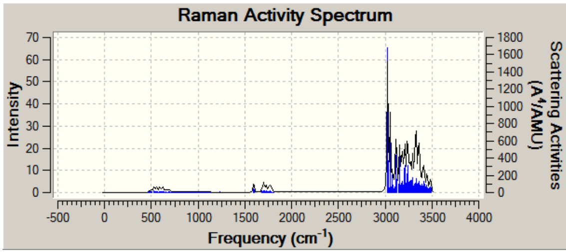

(b) 0.282 GPa

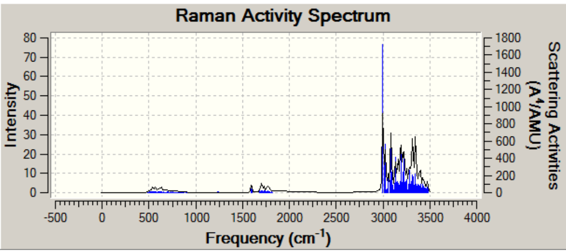

(c) 0.578 GPa

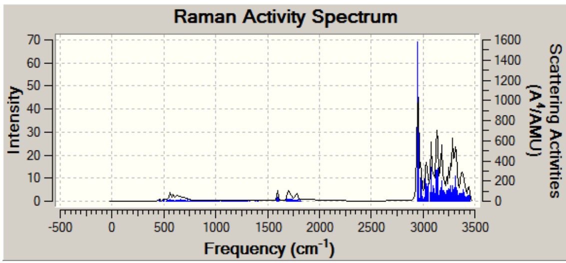

(d) 0.915 GPa

Figure 3.13: Computed Raman spectra of CH_4@sI

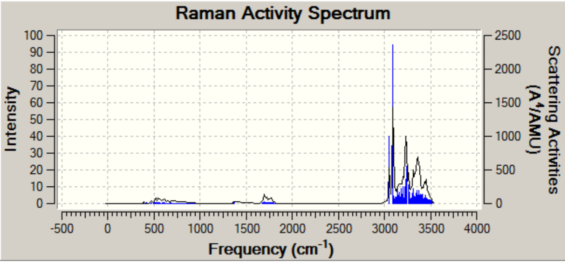

(a) 0.036 GPa

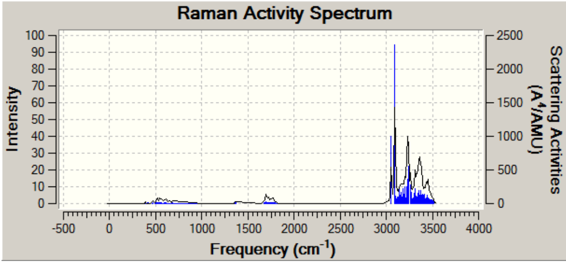

(b) 0.332 GPa

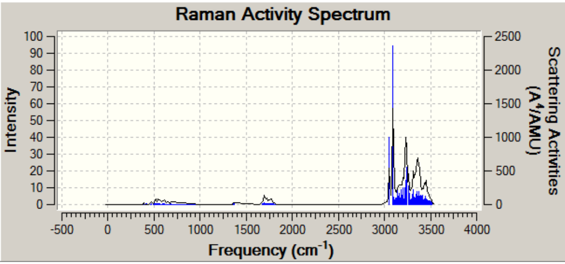

(c) 0.617 GPa

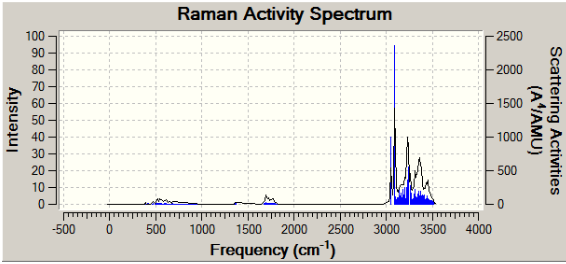

(d) 0.946 GPa

Figure 3.14: Computed Raman spectra of $CO_2@sI$

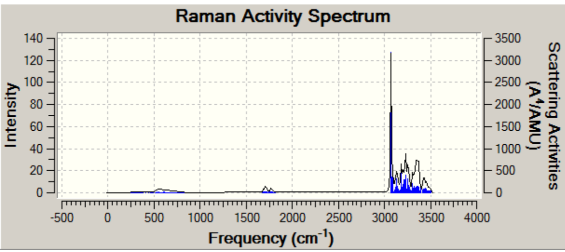

(a) 0.101 GPa

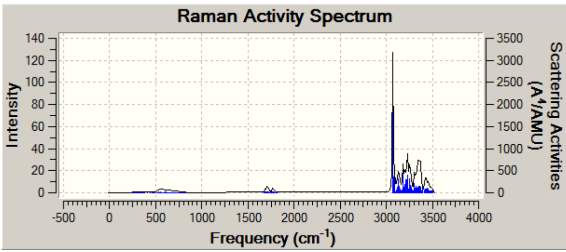

(b) 0.358 GPa

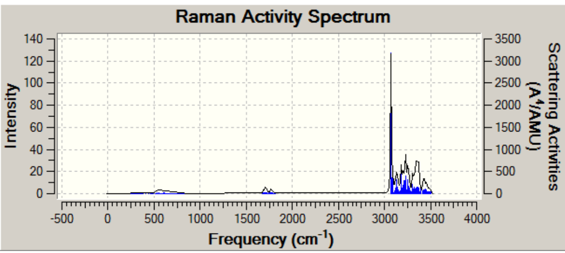

(c) 0.653 GPa

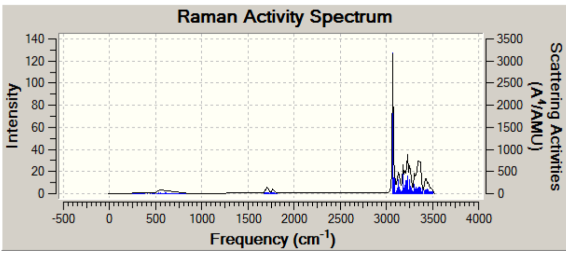

(d) 0.972 GPa

Figure 3.15: Computed Raman spectra of the empty clathrate

CHAPTER 4

CONCLUSIONES

1. Los clatratos hidratos de gas son sistemas químico físicos con implicaciones de mucho interés en áreas tan diversas como la planetología o la explotación de recursos naturales. La recreación en el laboratorio de las condiciones experimentales para la síntesis y caracterización de estos sistemas y la simulación computacional de modelos que describan fiablemente su comportamiento son imprescindibles para profundizar en el conocimiento de los mismos. Los cálculos mecánico-cuánticos estáticos discutidos en esta Tesis de Máster proporcionan una razonable aproximación a un conjunto de propiedades estructurales, energéticas y vibracionales, incluyendo efectos de presión hidrostática, de la fase sI de los clatratos hidratos de metano y dióxido de carbono.

2. Los clatratos vacíos sI y conteniendo metano o dióxido de carbono en todas sus cavidades muestran parámetros estructurales muy similares. El armazón de oxígeno que soporta la estructura presenta distancias promedio O-O más próximas en torno a 2.70 Å, en muy buen acuerdo con numerosos datos experimentales. Es interesante señalar que las optimizaciones geométricas llevadas a cabo utilizando una celda triclínica conducen a una estructura de equilibrio con una simetría prácticamente cúbica y un parámetro de red y unas posiciones atómicas en buen acuerdo también con los datos experimentales disponibles.

3. El estudio energético exhaustivo de las posibles orientaciones de las moléculas CH_4 y CO_2 en los dos tipos de cavidades, P y H, informa de distintos com-

portamientos. Así, las moléculas de metano pueden rotar libremente en las cavidades (tal y como se observa experimentalmente) pues las barreras energéticas no superan los 0.5 kcal/mol. Para el dióxido de carbono, la diferencia energética entre las configuraciones más y menos favorables es del orden de 6 kcal/mol. Encontramos una configuración de equilibrio con la molécula de CO_2 en el plano ecuatorial paralelo a los hexágonos de la caja H, y con la molécula de CO_2 en una dirección perpendicular a dos caras pentagonales paralelas cuando se aloja en una caja P. Las diferencias energéticas son debidas a la contribución estérica desestabilizante de la energía de interacción y no a la contribución estabilizante de la energía de dispersión que es muy similar en todas las configuraciones.

4. La ocupación progresiva de las cavidades P y H, bien por moléculas de CH_4 bien por moléculas de CO_2, es un proceso energético favorable. Al llegar a la saturación, la energía liberada es del orden de 47 kcal/mol en los dos sistemas. Sin embargo, hemos detectado de nuevo diferencias entre el metano y el dióxido de carbono. En el primer caso no existen preferencias por la ocupación de una caja P o H, siendo la energía liberada en la ocupación de una cavidad del orden de 5.7 kcal/mol, en acuerdo con datos experimentales. El dióxido de carbono prefiere la ocupación de una cavidad H, pues se libera en este proceso del orden de 6.0 kcal/mol frente a 4.6 kcal/mol cuando ocupa una cavidad P. El análisis de estos resultados utilizando modelos de cluster y modelos periódicos conduce a proponer efectos del entorno cristalino (posiblemente electrostáticos) que expliquen resultados discrepantes obtenidos con ambas metodologás.

5. Las ecuaciones de estado de los tres sistemas estudiados informan de estructuras cristalinas muy compresibles con valores del bulk modulus a presión cero de 16.5 GPa, 16.2 GPa y 15.7 GPa para el CH_4@sI, CO_2@sI y sI, respectivamente. Se lleva a cabo una descomposición de la compresibilidad de los cristales en términos de las compresibilidades de cada tipo de caja. Este analisis permite identificar a las cajas H como las que siguen en mayor medida el comportamiento macroscópico dado su mayor grado de ocupación en la celda unidad y su mayor compresibilidad en comparación con las cajas P.

6. La presión produce un efecto estabilizante que favorece la formación de los dos clatratos con una mayor preferencia en promedio para el sistema CH_4@sI.

7. El estudio del gradiente reducido de la densidad electrónica en los distintos tipos de caja y con presión nos ha permitido visualizar la relevancia de la dispersión en la estabilización de los complejos, así como los puentes de hidrógeno que mantienen la estructura del clatrato. El efecto de la presión es aumentar dichas superficies e incrementar la fuerza de los puentes de hidrógeno, que se ven desplazados hacia mayores densidades. Este último efecto es aún más destacado en el caso del CO_2 debido a la distorsión introducida por la presión. El estudio de la estabilidad con NCI nos ha permitido comprobar que las interacciones direccionales no están favorecidas. Completando este análisis con los de partición energética comprobamos que esto es debido a que dan lugar a mayores repulsiones estéricas.

8. Los modos simétricos y antismétricos de tensión de las moléculas huesped sufren desplazamiento al azul al pasar a estar encapsuladas. La magnitud del desplazamiento es mayor en el caso de las cajas P que en el caso de las cajas H. La presión no tiene un impacto considerable en el espectro vibracional salvo el desplazamiento hacia el rojo que sufren las frecuencias de tensión OH de las moléculas de agua.

9. Aunque nos ciñamos a las propiedades discutidas en esta Tesis de Máster, está claro que quedan abiertas varias cuestiones. Fundamentalmete, es necesario profundizar en los efectos de la red analizando el potencial electrostático en el entorno inmediato de la molécula gaseosa para poder llevar a cabo simulaciones fiables con modelos de cluster. También es necesario refinar los cálculos de energía total para poder proponer parámetros precisos de ecuaciones de estado tanto para los cristales como para las cavidades. Finalmente, debemos analizar con mayor detalle los espectros vibracionales obtenidos con el fin de llevar a cabo comparaciones rigurosas con resultados de otros cálculos y datos de investigaciones experimentales.

APPENDIX A

ATOMIC COORDINATES OF SI, CH_4@SI, AND CO_2@SI HYDRATES

In the next pages, we collect the the tables with the experimental [70] and optimized coordinates for each clathrate.

Atom	X	Y	Z	X	Y	Z	X	Y	Z	X	Y	Z
O	0.5000	0.5000	0.7500	0.5000	0.5000	0.2500	0.2500	0.0000	0.5000	0.7500	0.0000	0.5000
O	0.0000	0.7500	0.0000	0.0000	0.2500	0.0000	0.6837	0.1837	0.1837	0.3163	0.8163	0.8163
O	0.3163	0.8163	0.1837	0.6837	0.1837	0.8163	0.3163	0.1837	0.8163	0.6837	0.8163	0.1837
O	0.6837	0.8163	0.8163	0.3163	0.1837	0.1837	0.1837	0.6837	0.3163	0.8163	0.3163	0.6837
O	0.8163	0.3163	0.3163	0.1837	0.6837	0.6837	0.1837	0.3163	0.6837	0.8163	0.6837	0.3163
O	0.8163	0.6837	0.6837	0.1837	0.3163	0.3163	0.5000	0.3100	0.1142	0.5000	0.6900	0.8858
O	0.5000	0.6900	0.1142	0.5000	0.3100	0.8858	0.6142	0.0000	0.3100	0.3858	0.0000	0.6900
O	0.6142	0.0000	0.6900	0.3858	0.0000	0.3100	0.8100	0.1142	0.0000	0.1900	0.8858	0.0000
O	0.1900	0.1142	0.0000	0.8100	0.8858	0.0000	0.3100	0.5000	0.3858	0.6900	0.5000	0.6142
O	0.6900	0.5000	0.3858	0.3100	0.5000	0.6142	0.0000	0.6142	0.1900	0.0000	0.3858	0.8100
O	0.0000	0.6142	0.8100	0.0000	0.3858	0.1900	0.1142	0.8100	0.5000	0.8858	0.1900	0.5000
O	0.1142	0.1900	0.5000	0.8858	0.8100	0.5000	–	–	–	–	–	–

Table A.1: Experimental coordinates of the oxygen atoms in CH_4@sI hydrate

Atom	X	Y	Z	X	Y	Z	X	Y	Z	X	Y	Z
O	0.3840	0.9991	0.3090	0.8162	0.6845	0.6836	0.6166	0.0026	0.3097	0.1850	0.6825	0.6846
O	0.6149	0.9974	0.6912	0.1825	0.6842	0.3187	0.3820	0.0008	0.6918	0.8167	0.6836	0.3187
O	0.7496	0.0009	0.5008	0.4988	0.6900	0.8846	0.2496	0.0004	0.4995	0.5012	0.6898	0.1174
O	0.4995	0.4980	0.2494	0.4991	0.3079	0.8832	0.5011	0.4995	0.7505	0.5014	0.3067	0.1162
O	0.6913	0.4990	0.3820	0.8146	0.3174	0.6826	0.3093	0.5010	0.3838	0.1825	0.3154	0.6818
O	0.3101	0.4981	0.6169	0.1843	0.3181	0.3145	0.6912	0.5020	0.6154	0.8194	0.3180	0.3150
O	0.6861	0.1837	0.1818	0.8096	0.1158	0.9968	0.3176	0.1826	0.1837	0.1906	0.1161	0.0012
O	0.3150	0.1840	0.8173	0.9990	0.3832	0.8058	0.6817	0.1823	0.8151	0.0019	0.3851	0.1880
O	0.1163	0.1919	0.4966	0.0000	0.6169	0.8085	0.8834	0.1922	0.4995	0.9995	0.6177	0.1927
O	0.1163	0.8093	0.5025	0.1902	0.8826	0.0018	0.8835	0.8105	0.5006	0.8078	0.8826	0.0017
O	0.6828	0.8173	0.1857	0.0001	0.2504	0.9973	0.3172	0.8153	0.1842	0.9991	0.7489	0.0005
O	0.3166	0.8172	0.8186	0.6822	0.8153	0.8184	–	–	–	–	–	–
H	0.4692	0.9992	0.3168	0.7631	0.2688	0.7311	0.3000	0.0019	0.4303	0.7633	0.1399	0.9287
H	0.3456	0.1154	0.2294	0.0311	0.1846	0.4960	0.3637	0.9293	0.2633	0.1548	0.2702	0.6142
H	0.6633	0.0024	0.3817	0.1378	0.2390	0.4281	0.6431	0.0703	0.2641	0.8582	0.2377	0.5678
H	0.6582	0.8845	0.2332	0.8464	0.2712	0.3819	0.5296	0.9973	0.6839	0.9688	0.8173	0.5008
H	0.6994	0.9972	0.5700	0.1425	0.7642	0.5707	0.6535	0.1153	0.7695	0.1546	0.7303	0.3856
H	0.6354	0.9293	0.7392	0.8415	0.7327	0.6172	0.3356	0.0020	0.6198	0.8628	0.7629	0.4322
H	0.3576	0.0698	0.7367	0.7327	0.7689	0.2362	0.3399	0.8865	0.7734	0.5692	0.7352	0.1435
H	0.8366	0.1203	0.5011	0.7625	0.8628	0.0719	0.7999	0.9316	0.5023	0.2685	0.7656	0.2345
H	0.1997	0.0699	0.4959	0.3839	0.7671	0.1597	0.1631	0.8811	0.5016	0.2354	0.8566	0.0700
H	0.6195	0.4967	0.3354	0.2352	0.7313	0.7344	0.4302	0.4966	0.2996	0.4305	0.7377	0.8642
H	0.5013	0.6176	0.1636	0.2696	0.8446	0.8851	0.4971	0.4283	0.1996	0.7666	0.7344	0.7329
H	0.3819	0.4975	0.6637	0.6155	0.7694	0.8467	0.5702	0.5032	0.7001	0.7263	0.8409	0.8876
H	0.5020	0.5691	0.8005	0.9326	0.6417	0.7615	0.5000	0.3800	0.8368	0.0689	0.6399	0.7629
H	0.6836	0.5022	0.5301	0.1138	0.6596	0.2737	0.7712	0.6145	0.3418	0.8826	0.6555	0.2715
H	0.7375	0.4308	0.3580	0.4987	0.6826	0.9701	0.3170	0.5008	0.4692	0.5016	0.3147	0.0309
H	0.2623	0.5699	0.3637	0.9287	0.3620	0.7612	0.2313	0.3847	0.3412	0.1130	0.3415	0.7249
H	0.2326	0.6155	0.6599	0.0719	0.3617	0.2319	0.2647	0.4295	0.6410	0.8886	0.3421	0.2704
H	0.7375	0.5713	0.6361	0.8158	0.9678	0.0010	0.7678	0.3846	0.6569	0.8812	0.1627	0.9946
H	0.5719	0.2623	0.1366	0.1830	0.0308	0.0029	0.7373	0.2334	0.2297	0.0695	0.2003	0.9961
H	0.7332	0.1584	0.1147	0.9983	0.4687	0.8120	0.3870	0.2257	0.1576	0.0029	0.3002	0.9276
H	0.2363	0.2690	0.2668	0.0007	0.5333	0.1785	0.2374	0.1375	0.0699	0.0025	0.3380	0.1164
H	0.4288	0.2649	0.8593	0.9973	0.7013	0.9291	0.2631	0.2320	0.7684	0.9986	0.6591	0.1176
H	0.2682	0.1577	0.8843	0.1183	0.8359	0.0018	0.6127	0.2266	0.8402	0.9296	0.7989	0.9992

Table A.2: Calculated coordinates of oxygen and hydrogen atoms in sI

Atom	X	Y	Z	X	Y	Z	X	Y	Z	X	Y	Z
O	0.3873	0.9965	0.3083	0.6821	0.8217	0.8234	0.6219	0.9827	0.3089	0.8137	0.6868	0.6938
O	0.6133	0.9996	0.6929	0.1865	0.6960	0.7011	0.3793	0.0136	0.6911	0.1834	0.6788	0.3287
O	0.7522	0.9956	0.5038	0.8246	0.6705	0.3339	0.2476	0.0059	0.4968	0.4979	0.6940	0.8916
O	0.5005	0.4851	0.2478	0.5015	0.6831	0.1246	0.4991	0.5127	0.7538	0.5011	0.3136	0.8747
O	0.6925	0.4839	0.3839	0.5048	0.3023	0.1091	0.3095	0.4962	0.3845	0.8155	0.3224	0.6719
O	0.3072	0.5189	0.6177	0.1772	0.3321	0.6666	0.6918	0.5077	0.6178	0.1843	0.3150	0.3033
O	0.6796	0.1654	0.1723	0.8082	0.3061	0.3009	0.3193	0.1785	0.1801	0.8096	0.1092	0.9870
O	0.3090	0.1990	0.8024	0.1889	0.1209	0.9943	0.6820	0.1871	0.8070	0.9978	0.3876	0.8007
O	0.1155	0.1930	0.4912	0.9970	0.3838	0.1771	0.8793	0.1909	0.4919	0.9991	0.6173	0.8215
O	0.1202	0.8103	0.5070	0.0022	0.6128	0.1984	0.8851	0.8107	0.5065	0.1917	0.8899	0.0108
O	0.6942	0.8003	0.1921	0.8132	0.8793	0.0070	0.3197	0.8120	0.1912	0.9966	0.2492	0.9913
O	0.3244	0.8323	0.8295	0.0044	0.7500	0.0093	–	–	–	–	–	–
H	0.4733	0.9940	0.3173	0.7647	0.2726	0.7227	0.3000	0.0064	0.4280	0.7631	0.1378	0.9203
H	0.3479	0.1126	0.2265	0.0292	0.1857	0.4914	0.3654	0.9263	0.2658	0.1504	0.2819	0.6032
H	0.6665	0.9899	0.3821	0.1362	0.2380	0.4197	0.6448	0.0502	0.2601	0.8553	0.2386	0.5576
H	0.6663	0.8651	0.2381	0.8380	0.2624	0.3691	0.5271	0.0005	0.6859	0.9716	0.8166	0.5065
H	0.6999	0.9933	0.5725	0.1448	0.7707	0.5798	0.6512	0.1201	0.7647	0.1565	0.7261	0.3940
H	0.6331	0.9333	0.7437	0.8439	0.7345	0.6276	0.3330	0.0093	0.6186	0.8645	0.7596	0.4419
H	0.3537	0.0836	0.7306	0.7423	0.7535	0.2455	0.3440	0.9005	0.7803	0.5733	0.7246	0.1495
H	0.8334	0.1186	0.4991	0.7686	0.8550	0.0779	0.8021	0.9274	0.5080	0.2688	0.7620	0.2410
H	0.1982	0.0743	0.4911	0.3855	0.7643	0.1665	0.1659	0.8828	0.5024	0.2376	0.8613	0.0781
H	0.6205	0.4862	0.3366	0.2395	0.7440	0.7482	0.4302	0.4846	0.2979	0.4319	0.7443	0.8723
H	0.5016	0.6091	0.1674	0.2749	0.8571	0.8949	0.4979	0.4172	0.1978	0.7652	0.7377	0.7412
H	0.3793	0.5139	0.6648	0.6159	0.7735	0.8533	0.5688	0.5146	0.7029	0.7300	0.8420	0.8922
H	0.5023	0.5802	0.8043	0.9321	0.6437	0.7743	0.5014	0.3881	0.8327	0.0692	0.6446	0.7771
H	0.6851	0.5049	0.5322	0.1143	0.6569	0.2818	0.7758	0.6017	0.3522	0.8892	0.6460	0.2831
H	0.7359	0.4172	0.3556	0.4982	0.6844	0.9777	0.3193	0.5006	0.4699	0.5035	0.3123	0.0232
H	0.2633	0.5644	0.3637	0.9273	0.3667	0.7551	0.2314	0.3791	0.3338	0.1079	0.3514	0.7139
H	0.2334	0.6328	0.6712	0.0657	0.3595	0.2227	0.2609	0.4487	0.6367	0.8781	0.3340	0.2569
H	0.7382	0.5770	0.6383	0.8169	0.9635	0.0036	0.7681	0.3898	0.6515	0.8802	0.1599	0.9890
H	0.5727	0.2537	0.1274	0.1826	0.0368	0.9995	0.7296	0.2170	0.2198	0.0673	0.2019	0.9909
H	0.7290	0.1448	0.1052	0.9967	0.4714	0.8108	0.3893	0.2224	0.1519	0.9998	0.2988	0.9207
H	0.2374	0.2667	0.2579	0.0010	0.5311	0.1787	0.2366	0.1427	0.0625	0.9980	0.3365	0.1063
H	0.4287	0.2734	0.8496	0.0014	0.7022	0.9389	0.2573	0.2477	0.7546	0.0015	0.6598	0.1254
H	0.2633	0.1717	0.8708	0.1213	0.8390	0.0084	0.6139	0.2317	0.8326	0.9344	0.7981	0.0063

Table A.3: Calculated coordinates of oxygen and hydrogen atoms in $CO_2@sI$

Atom	X	Y	Z	X	Y	Z	X	Y	Z	X	Y	Z
O	0.3832	0.0002	0.3078	0.6829	0.8156	0.8177	0.6162	0.0027	0.3088	0.8159	0.6842	0.6839
O	0.6161	0.9991	0.6925	0.1849	0.6830	0.6847	0.3820	0.0010	0.6920	0.1832	0.6844	0.3184
O	0.7495	0.0012	0.5004	0.8156	0.6844	0.3182	0.2496	0.0000	0.5000	0.4991	0.6899	0.8840
O	0.5000	0.4982	0.2493	0.5011	0.6901	0.1176	0.5005	0.4990	0.7502	0.4993	0.3078	0.8836
O	0.6922	0.4988	0.3821	0.5009	0.3073	0.1168	0.3086	0.4998	0.3831	0.8158	0.3166	0.6828
O	0.3091	0.4981	0.6169	0.1829	0.3150	0.6823	0.6922	0.5010	0.6162	0.1830	0.3175	0.3146
O	0.6858	0.1844	0.1820	0.8187	0.3174	0.3144	0.3165	0.1841	0.1837	0.8101	0.1161	0.9965
O	0.3149	0.1843	0.8172	0.1901	0.1163	0.0010	0.6827	0.1833	0.8156	0.9991	0.3827	0.8062
O	0.1170	0.1915	0.4974	0.0014	0.3858	0.1882	0.8829	0.1921	0.4993	0.9999	0.6172	0.8090
O	0.1162	0.8090	0.5019	0.9996	0.6180	0.1932	0.8830	0.8105	0.5007	0.1908	0.8829	0.0013
O	0.6822	0.8172	0.1854	0.8077	0.8818	0.0013	0.3171	0.8162	0.1845	0.9997	0.2506	0.9980
O	0.3166	0.8164	0.8180	0.9995	0.7490	0.0010	–	–	–	–	–	–
H	0.4686	0.0000	0.3154	0.7639	0.2682	0.7317	0.2999	0.0020	0.4304	0.7639	0.1407	0.9284
H	0.3445	0.1171	0.2298	0.0319	0.1837	0.4965	0.3628	0.9304	0.2622	0.1554	0.2699	0.6147
H	0.6625	0.0026	0.3809	0.1384	0.2383	0.4283	0.6428	0.0706	0.2634	0.8579	0.2375	0.5680
H	0.6577	0.8847	0.2325	0.8459	0.2710	0.3813	0.5308	0.9985	0.6849	0.9685	0.8171	0.5007
H	0.6997	0.9980	0.5704	0.1425	0.7643	0.5703	0.6546	0.1161	0.7703	0.1553	0.7304	0.3856
H	0.6365	0.9305	0.7399	0.8412	0.7323	0.6172	0.3358	0.0020	0.6197	0.8625	0.7632	0.4322
H	0.3571	0.0702	0.7362	0.7321	0.7692	0.2363	0.3399	0.8861	0.7734	0.5691	0.7353	0.1440
H	0.8353	0.1207	0.5008	0.7620	0.8621	0.0717	0.8000	0.9319	0.5022	0.2681	0.7661	0.2346
H	0.1998	0.0696	0.4967	0.3838	0.7679	0.1600	0.1628	0.8810	0.5012	0.2358	0.8572	0.0698
H	0.6201	0.4964	0.3361	0.2353	0.7316	0.7344	0.4303	0.4966	0.2993	0.4304	0.7372	0.8636
H	0.5010	0.6179	0.1641	0.2697	0.8437	0.8849	0.4976	0.4287	0.1994	0.7663	0.7345	0.7332
H	0.3810	0.4974	0.6634	0.6158	0.7699	0.8458	0.5700	0.5025	0.6999	0.7267	0.8406	0.8871
H	0.5015	0.5687	0.7999	0.9321	0.6420	0.7625	0.5000	0.3800	0.8372	0.0686	0.6404	0.7628
H	0.6850	0.5017	0.5308	0.1142	0.6598	0.2741	0.7704	0.6151	0.3415	0.8815	0.6564	0.2707
H	0.7384	0.4307	0.3576	0.4992	0.6826	0.9695	0.3163	0.4998	0.4685	0.5013	0.3148	0.0313
H	0.2623	0.5692	0.3628	0.9291	0.3613	0.7613	0.2298	0.3843	0.3410	0.1131	0.3410	0.7254
H	0.2324	0.6158	0.6603	0.0710	0.3618	0.2324	0.2638	0.4294	0.6414	0.8882	0.3419	0.2697
H	0.7377	0.5707	0.6369	0.8158	0.9669	0.0007	0.7692	0.3841	0.6575	0.8814	0.1637	0.9949
H	0.5713	0.2625	0.1372	0.1831	0.0309	0.0026	0.7371	0.2337	0.2299	0.0690	0.2002	0.9965
H	0.7331	0.1590	0.1149	0.9980	0.4681	0.8123	0.3863	0.2273	0.1578	0.0026	0.3003	0.9280
H	0.2352	0.2692	0.2661	0.0003	0.5335	0.1791	0.2369	0.1376	0.0695	0.0022	0.3389	0.1165
H	0.4290	0.2649	0.8596	0.9978	0.7015	0.9295	0.2630	0.2326	0.7683	0.9990	0.6592	0.1177
H	0.2678	0.1581	0.8843	0.1187	0.8365	0.0018	0.6132	0.2273	0.8406	0.9297	0.7988	0.9994

Table A.4: Calculated coordinates of oxygen and hydrogen atoms in $CH_4@sI$

BIBLIOGRAPHY

[1] Buffett, B. A. *Annual Review of Earth and Planetary Sciences* **2000**, *28*, 477.

[2] Prieto-Ballesteros, O. In *Materia a Alta Presión. Fundamentos y Aplicaciones*; Menéndez, J. M., Aguado, F., Valiente, R., Recio, J. M., Eds.; Servicio de Publicaciones de la Universidad de Oviedo, 2011.

[3] Loveday, J. S.; Nelmes, R. J.; Guthrie, M.; Belmonte, S. A.; Allan, D. R.; Klug, D. D.; Tse, J. S.; Handa, Y. P. *Nature* **2001**, *410*, 661.

[4] Zhao, Y.; Xu, H.; Daemen, L. L.; Lokshin, K.; Tait, K. T.; Mao, W. L.; Luo, J.; Currier, R. P.; Hickmott, D. *PNAS* **2007**, *104*, 5787.

[5] Tulk, C. A.; Klug, D. D.; dos Santos, A. M.; Karotis, G.; Guthrie, M.; Molaison, J. J.; Pradhan, N. *The Journal of Chemical Physics* **2012**, *136*, 054502.

[6] Sloan, E. D.; Koh, C. A. *Clathrate hydrates of natural gases*; CRC Press, 2008.

[7] Loveday, J. S.; Nelmes, R. J. *Physical Chemistry Chemical Physics* **2008**, *10*, 937.

[8] Tse, J.; Shpakov, V. P.; Belosludov, V. R.; Trouw, F.; Handa, Y. P.; Press, W. *Europhys. Lett.* **2001**, *54*, 354.

[9] DiLabio, G. A.; Otero-de-la Roza, A. In *Reviews in Computational Chemistry*; Lipkowitz, K. B., Ed.; Wiley-VCH, Hoboken, NJ, 2014; (in press).

[10] Johnson, E. R.; Mackie, I. D.; DiLabio, G. A. *J. Phys. Org. Chem.* **2009**, *22*, 1127–1135.

[11] Santra, B.; Klime, J. c. v.; Alfè, D.; Tkatchenko, A.; Slater, B.; Michaelides, A.; Car, R.; Scheffler, M. *Phys. Rev. Lett.* **2011**, *107*, 185701.

[12] DiStasio Jr., R. A.; Santra, B.; Li, Z.; Wu, X.; Car, R. **2014**, preprint.

[13] Goerigk, L.; Kruse, H.; Grimme, S. *Chem. Phys. Chem.* **2011**, *12*, 3421.

[14] Kozuch, S.; Martin, J. M. L. *J. Chem. Theory Comput.* **2013**, *9*, 1918.

[15] Becke, A. D.; Johnson, E. R. *J. Chem. Phys.* **2007**, *127*, 154108.

[16] Otero-de-la Roza, A.; Johnson, E. R. *J. Chem. Phys.* **2013**, *138*, 204109.

[17] Otero-de-la Roza, A.; Johnson, E. R. *J. Chem. Phys.* **2012**, *136*, 174109.

[18] Otero-de-la Roza, A.; Johnson, E. R. *J. Chem. Phys.* **2012**, *137*, 054103.

[19] Otero-de-la Roza, A.; Cao, B. H.; Price, I. K.; Hein, J. E.; Johnson, E. R. *Angew. Chem. Int. Ed.* **2014**, (in press).

[20] Grimme, S. *J. Comp. Chem.* **2006**, *27*, 1787.

[21] Born, M.; Oppenheimer, J. R. *Annalen der Physik* **1927**, *389*, 457–484.

[22] Roothaan, C. C. J. *Reviews of Modern Physics* **1951**, *23*, 69–89.

[23] Roothaan, C. C. J. *Reviews of Modern Physics* **1960**, *32*, 179–185.

[24] Hohenberg, P.; Kohn, W. *Physical Review* **1964**, *136*, B864.

[25] Kohn, W.; Sham, L. J. *Physical Review* **1965**, *140*, A1133.

[26] Perdew, J. P.; Schmidt, K. *American Institute of Physics Conference Series*; American Institute of Physics Conference Series; 2001; Vol. 577; pp 1–20.

[27] Frisch, M. J. et al. *Gaussian 09*; Gaussian, Inc. , Wallingford CT, 2010; Vol. Revision B. 01.

[28] Becke, A. D. *J. Chem. Phys.* **1993**, *98*, 5648–5652.

[29] Lee, C.; Yang, W.; Parr, R. G. *Phys. Rev. B* **1988**, *37*, 785–789.

[30] Perdew, J. P.; Wang, Y. *Phys. Rev. B* **1986**, *33*, 8800.

[31] Perdew, J. P.; Burke, K.; Ernzerhof, M. *Phys. Rev. Lett.* **1996**, *77*, 3865.

[32] Perdew, J. P.; Burke, K.; Ernzerhof, M. *Phys. Rev. Lett.* **1996**, *78*, 1396.

[33] Becke, A. D. *Phys. Rev. A* **1988**, *38*, 3098.

[34] Burke, K. *J. Chem. Phys.* **2012**, *136*, 150901.

[35] Lacks, D. J.; Gordon, R. G. *Phys. Rev. A* **1993**, *47*, 4681.

[36] Kannemann, F. O.; Becke, A. D. *J. Chem. Theory Comput.* **2009**, *5*, 719–727.

[37] Dunning Jr., T. H. *J. Chem. Phys.* **1989**, 1007.

[38] Johnson, E. R.; Otero-de-la Roza, A.; Dale, S. G.; DiLabio, G. A. *J. Chem. Phys.* **2013**, *139*, 214109.

[39] Boys, S. F.; Bernardi, F. *Mol. Phys.* **1970**, *19*, 553.

[40] DiLabio, G. A.; Johnson, E. R.; Otero-de-la Roza, A. *Phys. Chem. Chem. Phys.* **2013**, *15*, 12821–12828.

[41] Becke, A. D.; Johnson, E. R. *J. Chem. Phys.* **2005**, *123*, 154101.

[42] Johnson, E. R.; Becke, A. D. *J. Chem. Phys.* **2006**, *124*, 174104.

[43] Grimme, S.; Antony, J.; Ehrlich, S.; Krieg, H. *J. Chem. Phys.* **2010**, *132*, 154104.

[44] Grimme, S.; Ehrlich, S.; Goerigk, L. *J. Comp. Chem.* **2011**, *32*, 1456.

[45] Otero-de-la Roza, A.; Johnson, E. R. *J. Chem. Phys.* **2013**, *138*, 054103.

[46] Becke, A. D.; Roussel, M. R. *Phys. Rev. A* **1989**, *39*, 3761.

[47] Barone, V.; Casarin, M.; Forrer, D.; Pavone, M.; Sambi, M.; Vittadini, A. *J. Comput. Chem.* **2009**, *30*, 934–939.

[48] Chai, J. D.; Head-Gordon, M. *Phys. Chem. Chem. Phys.* **2008**, *10*, 6615–6620.

[49] Giannozzi, P. et al. *J. Phys. Condens. Matter* **2009**, *21*, 395502.

[50] Arabi, A. A.; Becke, A. D. *J. Chem. Phys.* **2012**, *137*, 014104.

[51] Monkhorst, H. J.; Pack, J. D. *Phys. Rev. B* **1976**, *13*, 5188.

[52] Fletcher, R. *Practical Methods of Optimization*; Wiley, New York, 1980.

[53] Fenniri, H.; Packiarajan, M.; Vidale, K. L.; Sherman, D. M.; Hallenga, K.; Wood, K. V.; Stowell, J. G. *J. Am. Chem. Soc.* **2001**, *123*, 3854–3855.

[54] Kruse, P.; Johnson, E. R.; DiLabio, G. A.; Wolkow, R. A. *Nano Lett.* **2002**, *2*, 807–810.

[55] Sheiko, S. S.; Sun, F. C.; Randall, A.; Shirvanyants, D.; Rubinstein, M.; Lee, H.; Matyjaszewski, K. *Nature* **2006**, *440*, 191–194.

[56] DiLabio, G. A.; Piva, P. G.; Kruse, P.; Wolkow, R. A. *J. Am. Chem. Soc.* **2004**, *126*, 16048–16050.

[57] Bader, R. F. W. *Chem. Rev.* **1991**, *91*, 893–928.

[58] Bader, R. F. W. *Atoms in Molecules: A Quantum Theory.*; Oxford Science Publications, 1990.

[59] Matta, C. F.; Boyd, R. J. In *In The quantum theory of atoms in molecules.*; Matta, C. F., Boyd, R. J., Eds.; Wiley-VCH, 2007; pp 1–34.

[60] Becke, A. D.; Edgecombe, K. E. *J. Chem. Phys.* **1990**, *92*, 5397–5403.

[61] Silvi, B.; Savin, A. *Nature* **1994**, *371*, 683–686.

[62] Johnson, E. R.; Keinan, S.; Mori-Sanchez, P.; Contreras-Garcıa, J.; Cohen, A. J.; Yang, W. *J. Am. Chem. Soc.* **2010**, *132*, 6498.

[63] Arfken, G. *Mathematical Methods for Physicists*; Academic Press: Orlando, 1985.

[64] Contreras-García, J.; Johnson, E. R.; Keinan, S.; Chaudret, R.; Piquemal, J.-P.; Beratan, D. N.; Yang, W. *J. Chemp. Theory Comput.* **2011**, *7*, 625.

[65] Otero-de-la Roza, A.; Johnson, E. R.; Luaña, V. *Comp. Phys. Comm.* **2014**, *185*, 1007.

[66] Blanco, M. A.; Francisco, E.; Luaña, V. *Comp. Phys. Comm.* **2004**, *158*, 57.

[67] Otero-de-la Roza, A.; Luaña, V. *Comp. Phys. Comm.* **2011**, *182*, 1708.

[68] Otero-de-la Roza, A.; Abbasi-Pérez, D.; Luaña, V. *Comp. Phys. Comm.* **2011**, *182*, 2232.

[69] Wilson, E. B.; Decius, J. C.; Cross, P. C. *Molecular Vibrations: The Theory of Infrared and Raman Vibrational Spectra*; Dover Books on Chemistry, 1955.

[70] Kirchner, M. T.; Boese, R.; Billups, W. E.; Norman, L. R. *J. Am. Chem. Soc.* **2004**, *126*, 9407.

[71] Martin Pendas, A.; Costales, A.; Blanco, M. A.; Recio, J. M.; Luaña, V. *Phys. Rev. B* **2000**, *62*, 13970.

[72] Recio, J. M.; Franco, R.; Martin Pendas, A.; Blanco, M. A.; Pueyo, L.; Pandey, R. *Phys. Rev. B* **2001**, *63*, 184101.

[73] Armstrong, A.; Boto, R. A.; Dingwall, P.; Contreras-Garcia, J.; Harvey, M. J.; Mason, N.; Rzepa, H. S. *Chem. Science* **2014**, *5*, 2057.

[74] Baerends, E. et al. *ADF2010,SCM,Theoretical Chemistry*; Vrije Universiteit, Amsterdam,.

[75] Hiratsuka, M.; Ohmura, R.; Sum, A. K.; Yasuoka, K. *J. Chem. Phys.* **2012**, *136*, 044508.

[76] Ramya, K. R.; Pavan Kumar, G. V.; Venkatnathan, A. *J. Chem. Phys.* **2012**, *136*, 174305.

[77] Marion, A. *J. Chem. Phys.* **2014**, in press.

[78] Dartois, E.; Deboffle, D. *Astron. Astrophys.* **2008**, *490*, L19.